Title
INVESTIGATION OF ELECTRONIC AND NUCLEAR PROPERTIES OF SOME RARE EARTH ISOTOPES

Author
Budick, Burton.

Publication Date
1962-05-23

UCRL-10245

University of California

Ernest O. Lawrence Radiation Laboratory

Berkeley, California

DISCLAIMER

Research and Development

UCRL-10245
UC-34 Physics
TID-4500 (17th Ed.)

UNIVERSITY OF CALIFORNIA

Lawrence Radiation Laboratory
Berkeley, California

Contract No. W-7405-eng-48

INVESTIGATION OF ELECTRONIC AND NUCLEAR PROPERTIES OF SOME RARE EARTH ISOTOPES

Burton Budick

(Ph. D. Thesis)

May 23, 1962

Printed in USA. Price $2.00. Available from the
Office of Technical Services
U. S. Department of Commerce
Washington 25, D.C.

Contents

INVESTIGATION OF ELECTRONIC AND NUCLEAR PROPERTIES OF SOME RARE EARTH ISOTOPES

Burton Budick

Lawrence Radiation Laboratory
University of California
Berkeley, California

May 23, 1962

ABSTRACT

Electronic and nuclear properties of several rare earth isotopes have been investigated with the atomic-beam magnetic resonance technique. The spins of four isotopes have been found.

Isotope	$T_{1/2}$	I	J	Electronic State
Ho^{161}	2.5h	7/2	15/2	^4I
Er^{165}	9.8 h	5/2	6*	^3H
Pr^{143}	14 d	7/2	9/2*	^4I
Nd^{149}	1.8 h	5/2	4*	^5I

Asterisked quantities were determined by other experimenters, but were directly involved in this work. From the J-level assignment for holmium and its measured g_J value, we may infer an electronic configuration of $4f^{11}6s^2$.

The magnetic dipole and electric quadrupole interaction constants have been measured for two promethium isotopes.

Isotope	$T_{1/2}$	I	a	b	$g_J(J = 7/2)$	Electronic State
Pm^{147}	2.6 yr	7/2*	447(9)	-267(71)	-0.8283 (6)	^6H
Pm^{151}	27 h	5/2*	358(22)	-778(93)	-0.8272 (7)	^6H

A best-fit value for g_J was also found in analyzing the data. From the measurements, we may deduce values for the nuclear moments.

Isotope	μ (nm)	Q(b)
Pm^{147}	3.2 (3)	1.0 (3)
Pm^{151}	1.8 (2)	2.9 (4)

The interpretation of these results as well as a description of the technique used to obtain them form the subject of this thesis.

I. INTRODUCTION

This paper treats the standard topics encompassed by the broad title Atomic Beam Radio-Frequency Spectroscopy, as well as reporting some experimental results. The framework for the discussion is the language and techniques of perturbation theory.[1,2] Such an approach is adopted not only out of computational necessity but also because perturbation theory is an elegant way of keeping track of the physical situation. In its matrix mechanical form, perturbation theory keeps the physical interaction and the states affected by this interaction always in easy view. Actual calculation of matrix elements, especially by group theory, allows further insight into the symmetries of the problem.

Although the perturbation of degenerate states creates a rather formidable formalism,[1] the main conclusions can be drawn from an elementary treatment of the nondegenerate two-level system.

Let the unperturbed interaction and its eigenvectors be represented by $\mathcal{H}_0$ and $|1\rangle$, $|2\rangle$. The true interaction includes the perturbation $\mathcal{H}$ and has eigenvectors $|1'\rangle$, $|2'\rangle$. Thus

$$\left.\begin{aligned} &\mathcal{H}' = \mathcal{H}_0 + \mathcal{H} \\ &|1'\rangle = |1\rangle + a\,|2\rangle, \quad E_1' = E_1 + \Delta E_1; \\ &|2'\rangle = |2\rangle + b\,|1\rangle, \quad E_2' = E_2 + \Delta E_2 . \end{aligned}\right\} \tag{1}$$

Substituting in the new operator equation,

$$\mathcal{H}'\,|1'\rangle = E_1'\,|1'\rangle , \tag{2}$$

and bracketing with $\langle 1|$ and $\langle 2|$ gives

$$\left.\begin{aligned} \Delta E_1 &= \mathcal{H}_{11} + a\,\mathcal{H}_{12} , \\ \Delta E + \Delta E_1 &= \mathcal{H}_{22} + \frac{1}{a}\,\mathcal{H}_{21} , \end{aligned}\right\} \tag{3}$$

where $\mathcal{H}_{11} = \langle 1|\mathcal{H}|1\rangle$ and $\Delta E = E_1 - E_2$. For $\Delta E >> \Delta E_1$, $\Delta E >> \Delta E_2$, then from the second relation,

$$a = \frac{\mathcal{H}_{21}}{\Delta E} . \tag{4}$$

Putting this into the first equation immediately yields

$$\Delta E_1 = \mathcal{H}_{11} + \frac{|\mathcal{H}_{12}|^2}{\Delta E} , \tag{5}$$

and, to this order of the approximation,

$$|1'\rangle = |1\rangle + \frac{\mathcal{H}_{21}}{\Delta E} |2\rangle . \tag{6}$$

Even this crude analysis has revealed two important results. The perturbation approach is valid so long as the energy separation between perturbing levels is large compared with the magnitude of the actual perturbation. Secondly, a prescription is given for finding the new wave function. As expected, this new wave function is an admixture of the unperturbed functions, corresponding to the fact that the physical interaction has made it possible for the system to exist in both the old states.

For completeness the other important features of perturbation technique are quoted; the effect of the perturbation is to push the interacting energy levels apart, while the center of gravity is unshifted.

II. ELECTRONIC STRUCTURE

In this spirit we proceed to an analysis of electronic structure. With a Hamiltonian consisting of kinetic and electron-nucleus potential energy terms, the energy of the atom is specified as being that of a particular configuration. This corresponds to specifying the n,ℓ quantum numbers of each electron. The Coulomb repulsion between electrons creates a term structure, each term belonging to a pair of L, S values. The lowest term is given by Hund's Rule for equivalent electrons. (A proof of Hund's Rule is sketched in Appendix I.) Each of these terms is $(2L + 1)(2S + 1)$-fold degenerate, the degeneracy being removed by the spin-orbit interaction. In the rare-earth region this is conveniently treated as a perturbation which must leave the total electronic angular momentum invariant. Thus, the resultant level structure is specified by L, S, J, and each level is $(2J + 1)$-fold degenerate.

The total Hamiltonian and the effect of each of its terms are shown in Fig. 1, for Pm. To show the degree of validity of the perturbation approach I have included energy separations. The configuration separation is estimated from cerium,[3] the term separations were actually computed,[4] and the fine-structure separations were interpolated from neighboring elements.[5]

It is clear from the figure that the term separation is not small compared with the energy difference between configurations. In order to use perturbation theory one must make the central-field approximation, in which the Hamiltonian consists of kinetic energy terms and a spherically symmetric potential energy. The perturbation is then the difference between the true potential energy and the approximate spherically symmetric one.

$$H = \sum_i \frac{P_i^2}{2m} + \frac{Ze^2}{r_i} + \sum_{i>j} \frac{e^2}{r_{ij}} + \sum_i \xi_i \underset{\sim}{l}_i \cdot \underset{\sim}{s}_i$$

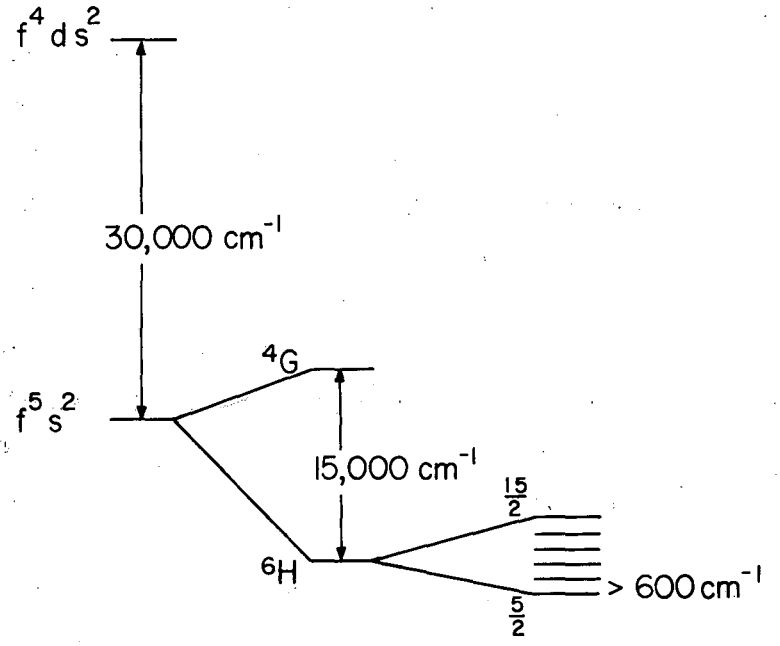

Fig. I. Electronic Structure of Promethium

MU-26749

Fig. 1. Electronic structure of promethium.

III. HYPERFINE STRUCTURE

In accordance with our first assumption, the criterion for the extension of perturbation theory to hfs is that the hfs interaction be small compared with the fine-structure separation. This may be taken as $a/\xi << 1$, where a and ξ are the hfs and fs constants respectively. In the rare earths a is of the order of hundreds of megacycles and ξ is about a thousand wave numbers, so the condition is fully met.

Before discussing the physical interaction that gives rise to the hfs phenomonon, I offer a brief historical note. The first explanation for the presence of hfs in the spectrum of a single isotope was put forth by Pauli,[6] who postulated the existence of a nuclear spin angular momentum and its associated magnetic moment. Fermi[7] and Hargreaves[8] worked out the implications of this magnetic moment for the case of S electrons. It appears that the first general treatment of hfs for many electron spectra was given by Goudsmit,[9] who used the method of sum rules. It has recently been pointed out that the magnetic dipole part of the hfs interaction is adequately accounted for by classical physics.[10] The modern treatment by Schwartz[11] is so thorough that all future work must rely heavily on it.

Schwartz essentially adopts the view, originally put forth by Casimir,[12] that the origin of hfs is in the deviation of the electron-nucleus interaction from that of a point charge coupled with the existence of a nuclear angular momentum. Thus electric and higher-order magnetic pole interactions may exist. Whatever the nature of these noncentral interactions, the perturbing Hamiltonian can be written

$$\mathcal{H} = \sum_k T_e^{(k)} \cdot T_N^{(k)} , \qquad (7)$$

where $T_e^{(k)}$ is a tensor operator in the space of electronic coordinates whose rank, k, is defined in terms of its commutation properties with the vector $\vec{J}$. The specific forms that this expression takes for the magnetic dipole interaction and the electric quadrupole interaction are

developed in Appendix II. They are

$$\mathcal{H}_{magn} = \frac{2\mu_0\mu_N g_I}{I} \left\langle \frac{1}{r^3} \right\rangle \sum_i \underset{\sim}{\ell}_i - \sqrt{10}\,(\underset{\sim}{s}\,\underset{\sim}{C}^2)_i \cdot \underset{\sim}{I}\,, \tag{8}$$

$$\mathcal{H}_{elec} = \sum_{e,N,q} (-)^q \frac{e^2 r_N^2}{r_e^3} C_q^2(\theta_e, \phi_e)\, C_{-q}^2(\theta_N, \phi_N), \tag{9}$$

where μ_0 and μ_N are the Bohr and nuclear magneton respectively and g_I is the nuclear g factor. Other moments for $K = 1, 2$ vanish because of the parity of the nuclear wave function.[13]

Within a manifold of states of a given J level the Wigner-Eckart theorem enables us to write

$$\frac{2\mu_0\mu_N g_I}{I} \left\langle \frac{1}{r^3} \right\rangle \sum_i \underset{\sim}{\ell}_i - \sqrt{10}\,(\underset{\sim}{s}\,\underset{\sim}{C}^2)_i \cdot \underset{\sim}{I} = a\,\underset{\sim}{J} \cdot \underset{\sim}{I}. \tag{10}$$

The proportionality constant a must be determined for each configuration separately, but a general result has been derived for a configuration of n equivalent electrons, angular momentum ℓ, coupling to the Hund's Rule ground state:[14]

$$a(J) = 2g_I\mu_0\,\mu_N \left\langle \frac{1}{r^3} \right\rangle \left\{ \frac{J(J+1) + L(L+1) - S(S+1)}{2J(J+1)} \right.$$

$$+ \frac{2(2L - n^2)}{n^2(2L-1)(2\ell-1)(2\ell+3)}$$

$$\left[\frac{L(L+1)\,[\,J(J+1) + S(S+1) - L(L+1)\,]}{2J(J+1)} \right. \tag{11}$$

$$\left. \left. - \frac{3}{4} \frac{[\,J(J+1) - L(L+1) - S(S+1)\,]\,[\,J(J+1) + L(L+1) - S(S+1)\,]}{J(J+1)} \right] \right\}.$$

It is worth noting that matrix elements of the magnetic hyperfine interaction (10) involve the cosine factor[15]

$$F(F+1) - J(J+1) - I(I+1) = (-1)^{-F-I-J} 2[J(J+1)(2J+1)I(I+1)(2I+1)]^{1/2} \times \begin{Bmatrix} F & J & I \\ 1 & I & J \end{Bmatrix} . \tag{12}$$

The electric quadrupole interaction can be written[16]

$$\mathcal{H}_{elec} = e^2 q_J Q \frac{3(\underset{\sim}{I}\cdot\underset{\sim}{J})^2 + \frac{3}{2}\underset{\sim}{I}\cdot\underset{\sim}{J} - I(I+1)J(J+1)}{2I(2I-1)J(2J-1)}$$

$$= b\, Q_{operator} . \tag{13}$$

This result follows immediately from (18) below. Referring to (9), we see

$$Q = \left\langle r_N^2 \right\rangle \left\langle I, I \left| 2C_{-q}^2 \right| I, I \right\rangle ,$$

$$q_J = -\left\langle \frac{1}{r^3} \right\rangle \left\langle JJ \left| 2C_q^2 \right| JJ \right\rangle .$$

Using these relations we may derive a general formula for $b = e^2 q_J Q$ for equivalent electrons similar to (11):

$$b = e^2 Q \left\langle \frac{1}{r_e^3} \right\rangle \frac{3K(K+1) - 4L(L+1)J(J+1)}{2L(2L-1)(J+1)(2J+3)} \frac{2L(2\ell - 2n + 1)}{N(2\ell+3)(2\ell-1)} , \tag{15}$$

where

$$K = S(S+1) - J(J+1) - L(L+1) .$$

The "cosine square" factor contained in $Q_{operator}$ and multiplying b can be written

$$Q_{operator} = (-1)^{-I-J-F} \frac{1}{4} \left[\frac{(I+1)(2I+1)(2I+3)(J+1)(2J+1)(2J+3)}{I(2I-1)J(2J-1)} \right]^{1/2} \begin{Bmatrix} F & I & J \\ 2 & J & I \end{Bmatrix} . \tag{16}$$

Having developed these formulae, we are now in a position to examine the significance of off-diagonal matrix elements between different fine-structure states as expressed in (5). That is, we can see how our perturbation approach breaks down when the fine structure is small. The hfs Hamiltonian consisting of (8) and (9) has matrix elements between different J levels:

$$\left\langle IJFm_F \left| \underset{\sim}{\ell} - \sqrt{10}\,(\underset{\sim}{s}\,\underset{\sim}{C}^2)^1 \right| IJ'Fm_F \right\rangle =$$

$$= (-1)^{I+J+F} \begin{Bmatrix} I & I & 1 \\ J' & J & F \end{Bmatrix} (I||I||I)(J||\underset{\sim}{\ell} - \sqrt{10}\,(\underset{\sim}{s}\,\underset{\sim}{C}^2)^1||J'), \qquad (17)$$

$$\left\langle IJFm_F \left| C_e^{\,2} \cdot C_N^{\,2} \right| IJ'Fm_F \right\rangle =$$

$$= (-1)^{I+J+F} \begin{Bmatrix} I & I & 2 \\ J' & J & F \end{Bmatrix} (I||C^2||I)(J||C^2||J') \,. \qquad (18)$$

When we square the matrix element $(J\,|\mathcal{H}_{hfs}|\,J')$ we get three terms, each containing a product of two 6-j symbols. Consider the dipole-dipole term,

$$\begin{Bmatrix} F & J' & I \\ 1 & I & J \end{Bmatrix} \begin{Bmatrix} F & J' & I \\ 1 & I & J \end{Bmatrix} =$$

$$= \sum_X (2X+1)\,(-)^{X+F+3I+2J+J'+2} \begin{Bmatrix} 1 & 1 & X \\ I & I & I \end{Bmatrix} \begin{Bmatrix} 1 & 1 & X \\ J & J & J' \end{Bmatrix} \begin{Bmatrix} F & J & I \\ X & I & J \end{Bmatrix} . \qquad (19)$$

The term with $X = 1$ has the same 6-j symbol as appears in (12) and therefore necessitates a correction to a (J). Setting $X = 2$ similarly gives a correction to b as seen from (16). There are analogous contributions from the dipole-quadrupole and quadrupole-quadrupole terms. These contributions have been tabulated.[17]

All our work thus far has been in the absence of a magnetic field. Under these circumstances space is isotropic as far as an isolated atom is concerned. The atom's rotational invariance implies that its total angular momentum F must be a good quantum number. In the presence of a magnetic field this is no longer true. We may think of the effect of the magnetic field in two ways. On the vector model the external field uncouples I and J from each other and couples them separately to the field axis. Rather weak fields suffice because I is coupled to J through the nuclear magnetic moment. Uncoupling occurs as a result of interaction of the much larger electronic magnetic moment with the external field. Alternatively, in line with our perturbation approach, we may think of the magnetic field as a perturbation through which the proximity of adjacent F levels is felt. As the Zeeman splitting becomes comparable with the separation between F states, first-order perturbation theory breaks down and we have intermediate coupling.

The perturbation Hamiltonian is

$$\mathcal{H} = - g_J \mu_0 \underset{\sim}{J} \cdot \underset{\sim}{H} - g_I \mu_0 \underset{\sim}{I} \cdot \underset{\sim}{H} . \tag{20}$$

For small enough fields--i.e., the Zeeman region of hfs--we require only the first-order perturbation result:

$$W_{F, m_F} = \left[-g_J \frac{F(F+1) + J(J+1) - I(I+1)}{2F(F+1)} - g_I \frac{F(F+1) + I(I+1) - J(J+1)}{2F(F+1)} \right] \mu_0 H m_F$$

$$= g_F \mu_0 m_F H . \tag{21}$$

If we neglect the term in g_I we may write

$$g_F \approx - g_J \frac{F(F+1) + J(J+1) - I(I+1)}{2F(F+1)} . \tag{22}$$

The second-order correction given in (5),

$$\frac{|\mathcal{H}_{12}|^2}{\Delta E} = \frac{\left| \left\langle IJFm_F \right| - \mu_J \cdot \underset{\sim}{H} - \mu_I \cdot \underset{\sim}{H} \left| IJF'm_F \right\rangle \right|^2}{h \Delta \nu_{FF'}} , \tag{23}$$

gives us "the handle" on the hfs. Matrix elements of this type are tabulated by Ramsey[16] and Millman.[18] Using tensor operator techniques, we have

$$\left\langle IJFm_F \left| J_Z \right| I'J'F'm_F' \right\rangle = (-1)^{F-m_F} \begin{pmatrix} F & 1 & F' \\ -m_F & 0 & m_F \end{pmatrix} (IJF \| J \| I'J'F') =$$

$$= (-1)^{F-m_F} \begin{pmatrix} F & 1 & F' \\ -m_F & 0 & m_F \end{pmatrix} \delta(I, I') \, (-1)^{J+F+I+1} \sqrt{(2F+1)(2F'+1)}$$

$$\times \begin{Bmatrix} F & I & F' \\ J' & I & J \end{Bmatrix} (J \| J \| J') \tag{24}$$

If the external field is increased until the Zeeman splitting is much greater than the hfs separations, the Paschen-Back region of hfs, then I and J precess independently about the field. Only their projections on the field axis have nonzero average values. Our expressions (10) and (13), together with the external field energy, give

$$W_{m_I m_J} = a m_I m_J + \frac{b}{4} \frac{[3m_J^2 - J(J+1)]\,[3m_I^2 - I(I+1)]}{J(2J-1)I(2I-1)} - g_J \mu_0 m_J H - g_I \mu_0 m_I H \, . \tag{25}$$

IV. APPARATUS AND TECHNIQUE

A. The Flop-In Geometry

Our discussion thus far has been concerned with atomic hfs and Zeeman splittings of free atoms. It has been pointed out above that these energy separations depend on the magnetic dipole moment and electric quadrupole moment of the nucleus. Atomic spectroscopy has, in addition, yielded information on octupole moments, proton structure, and the distribution of nuclear magnetism. It has provided the only tests of quantum electrodynamics in the form of the anomalous moment of the electron and the Lamb shift. In two of its more recent developments, optical pumping and masers, it promises to provide extremely accurate frequency standards and to permit investigation of excited states.

The technique we used--atomic beam magnetic resonance--was responsible for many of the discoveries mentioned above. It is among the most sophisticated and precise techniques of modern physics. To fully appreciate it one should trace its development from the introduction of the two-wire field in 1934 by Rabi[19] to the multiple rf loops of Ramsey. Rabi successfully employed the flop-out geometry in 1938.[20] The apparatus to be described is of the flop-in type introduced by Zacharias[21] to study rare isotopes. It further resembles the Zacharias machine in that it is asymmetric and is intended to flip moments of the order of a Bohr magneton. The C field is therefore typically set at hundreds rather than thousands of gauss. The apparatus shown in Fig. 2 has been completely described elsewhere.[22] Notable modifications of Brink's design include the oven loader[23] and the button holder.[24]

In the flop-in geometry the gradients of the A and B fields are set so that an atom emerging from the slit undergoes equal deflections in the same direction. Only atoms whose magnetic moments have reversed direction as a result of the radio-frequency resonance and which therefore undergo an equal but opposite deflection in the B magnet reach the detector slit. The geometry has thus imposed a selection rule, namely $\Delta m_J = \pm 1$. When this is combined with the quantum

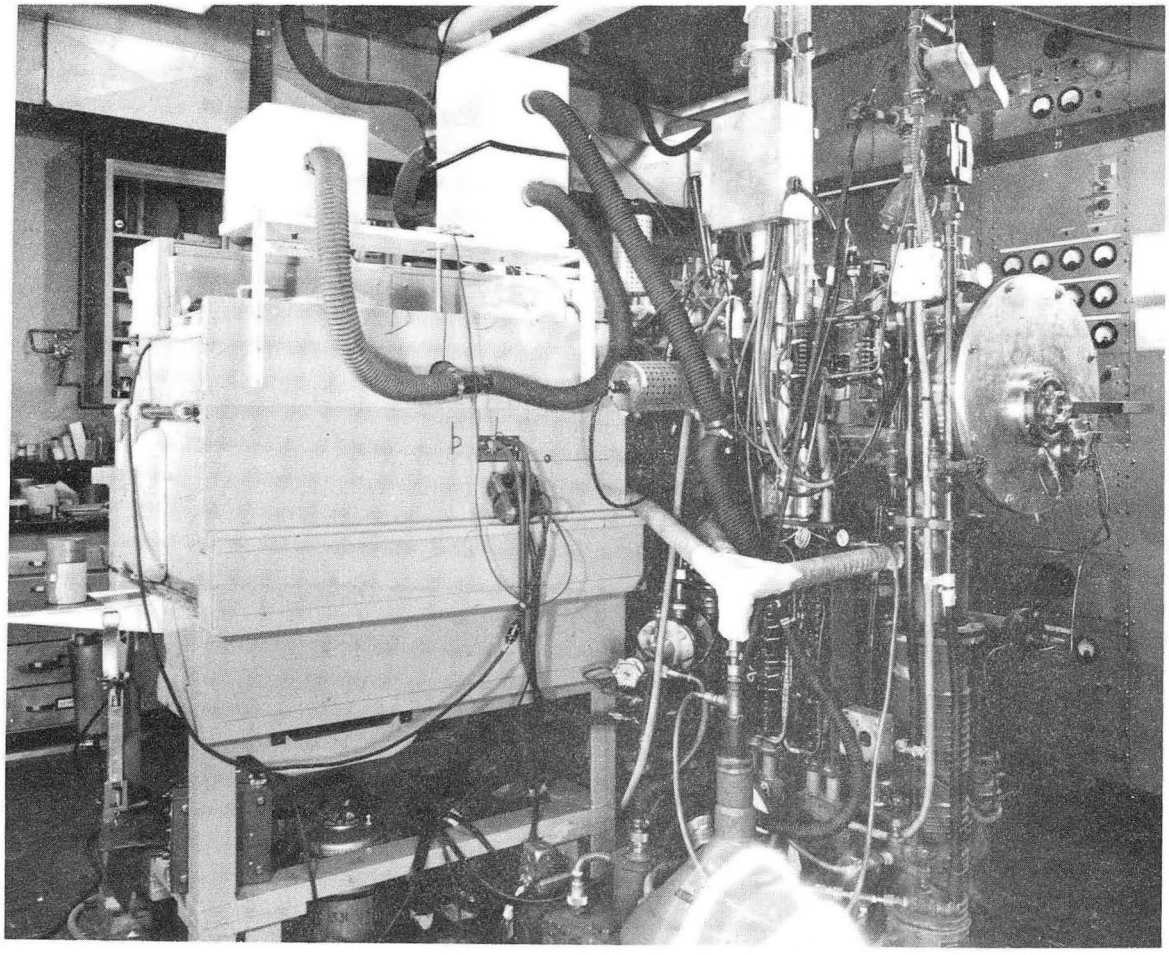

ZN-2591

Fig. 2. Atomic beam apparatus.

mechanical selection rules the number of observable transitions is sharply reduced. This reduction is compensated for by ease of identification.

B. The Transition Region and Selection Rules

To see what the quantum-mechanical selection rules are we must again invoke perturbation theory. In this case, however, we are dealing with time-dependent perturbation theory. We think of the perturbation, not as altering the energy states, but as causing transitions between them. Our interest is no longer in the energy shift, but rather in the transition probability.

The perturbing Hamiltonian is again given by Eq. (20), but with the static C field replaced by the oscillating radio-frequency field. If the rf field has a component in the z direction, as defined by the static field, then the selection rules $\Delta F = 0, \pm 1$, $\Delta m_F = 0$ follow immediately from the 3-j symbol in (24). If the rf field has components perpendicular to the static field we have

$$\left\langle IJFm_F \left| J_x \pm iJ_y \right| I'J'F'm_F' \right\rangle = (-1)^{F-m_F} \begin{pmatrix} F & 1 & F' \\ -m_F & \pm 1 & m_F \end{pmatrix} (IJF \| J \| I'J'F'), \tag{26}$$

and transitions with $\Delta m_F = \pm 1$ are now allowed.

The high-field selection rules are deduced from the matrix elements[1]

$$\begin{aligned} \left\langle m_J m_I \left| J_z \right| m_J m_I \right\rangle &= m_J , \\ \left\langle m_J+1 \; m_I \left| J_x + iJ_y \right| m_J m_I \right\rangle &= \sqrt{(J-m_J)(J+m_J+1)} , \\ \left\langle m_J-1 \; m_I \left| J_x - iJ_y \right| m_J m_I \right\rangle &= \sqrt{(J+m_J)(J-m_J+1)} . \end{aligned} \tag{27}$$

They are $\Delta m_J = 0, \pm 1$; $\Delta m_I = 0, \pm 1$.

The transition probability can be calculated in a variety of ways. In the first such calculation,[25] Rabi assumed that the system is quantized along a field axis while the field itself precesses about the z direction. Alternatively, it is a straightforward matter to apply first-order time-dependent perturbation theory with the perturbing Hamiltonian a function of time.[26] More recent methods transform the Hamiltonian so it is time-independent and use its basis functions in the time-dependent theory.[27] This procedure is more easily generalized to the case of multiple levels. Finally, there is the elegant technique of the rotating coordinate system, which reduces the problem to one of geometry.[28]

A loop of wire is used to set up the rf field. The ac through the wire is read and the field computed by use of the circuital law. Typical fields are of the order of hundreds of milligauss. A sketch of the loop together with a table of equipment used to generate the radio-frequency has been published.[24] The transition region is about 1 cm long. This dimension and the magnitude of the deflections in the inhomogeneous fields decide which portion of the velocity distribution will be used.

From Eqs. (21) and (23) it is clear that two simultaneous measurements must be made, one of the frequency and the other of the steady field. In order to make them of comparable precision, the magnetic field is calibrated in terms of the ($F = 2\ m_F = -1 \longleftrightarrow F=2\ m_F=-2$) transition in potassium-39. Potassium has a convenient hfs and its constants have been determined very accurately.[29] It is easily detected on a tungsten hot wire.

C. Detection

The ionization potential of most rare earth metals is too high to be detected on a hot wire. Advantage is taken of the radioactivity of the samples. Beams are collected on freshly flamed platinum foils and counted in β-counters operated as Geiger counters. The collection efficiency for platinum is close to 100%.[30]

D. Data Analysis

The high values of I and J encountered in the rare earth region make hand calculations prohibitive. Instead, two IBM programs have been constructed. The first,[31] designed for the IBM 704, performs a least-squares fit to a set of resonances. It requires as input information I, J, F_1, m_1, F_2, m_2, the transition frequency and its uncertainty, the magnetic field and its uncertainty, and rough values of a, b, g_J, and g_I. Any or all of the last four may be left free to vary. The computer prints out best-fit values together with energy levels, residuals, and the value of a function χ^2 which measures the goodness of fit. It is related to the standard deviation in a manner described by Fisher.[32]

The second routine actually diagonalizes the Hamiltonian and solves for the energy levels.[33] Its input is the same as above except, of course, for the field and frequency, which now appear in the output. In addition, this program designed for the IBM 650 prints out transition frequencies for positive and negative moments, the frequency divided by the field, and the derivative of the frequency with respect to the field.

V. PROMETHIUM-147

A. Background and Motivation

Promethium, atomic number 61, has no stable isotopes. An explanation of this anomaly on the basis of the nuclear shell model has been proposed.[34] The first positive chemical identification was made in 1947.[35] Pm^{147}, in particular, has been studied intensively. Its β spectrum has been measured accurately,[36] and although first-forbidden, exhibits the allowed shape.[37] There is evidence of a γ spectrum.[38] The nuclear spin and his incentive for measuring it are reported by Cabezas.[39] Klinkenberg has measured the spin and hfs, using optical spectroscopy.[40] While the atomic beam work was in progress a paramagnetic result also was reported in the literature.[41]

Interest in the hfs of Pm^{147} was stimulated by the possibility of measuring the hfs of Pm^{149} and Pm^{151}. This sequence of isotopes would occur in the transition region between the shell and collective

models. The problem took on added interest with the realization that the 89th and 90th neutrons were being added to form Pm^{151}. It is known from optical and nuclear spectroscopy that this pair of neutrons enhances collective effects. Evidence for this enhancement is found in isotope shifts, quadrupole moments, and transition probabilities.

B. Beam Production

Promethium is a fission product and has a 2.6-year half life. It is readily purchased in the form of the chloride in curie quantities. These apparent advantages are compensated for by the difficulty of "a chemistry." A spectroscopic analysis and a pulse-height spectrum showed that some shipments of Pm were contaminated with americium and with an isotope of samarium. On careful investigation it was established that neither of these could confuse the Pm results.

A huge excess of nitric acid was added to 1 curie of the chloride and the nitrate product reduced to about 1 ml. This was carefully pipetted into the oven inner liner and slowly heated to 700°F on a hot plate to form the oxide. As the oxidation state was unknown, two reducing agents were tried, carbon and misch metal. Both showed a limited success, the ratio of floppable atoms to nonfloppable ones never exceeding 3:1. In the later stages of the work misch metal was used exclusively. Despite the high beam intensities, 5000 counts/min was typical; the signal-to-noise ratio was barely 2:1 in intermediate field. This was the ultimate limiting factor. Attempts were made to improve this ratio by varying the rf power and the strengths of the A and B fields. Neither of these variations showed any effect.

C. Results

A schematic diagram of the hfs is shown in Fig. 3 and the four observable flop-in transitions indicated. The transition in the highest F state is designated as α, the next highest, β, and so on. Some resonance curves are shown in Figs. 4 and 5. Interestingly, the β and δ transitions coincided up to quite high values of the field. With the exception of some low-field points in the linear Zeeman region, all the observed transitions are listed in Table I. The table also compares theory with experiment by juxtaposing the calculated transition frequencies and the observed ones. The best-fit values for the constants are

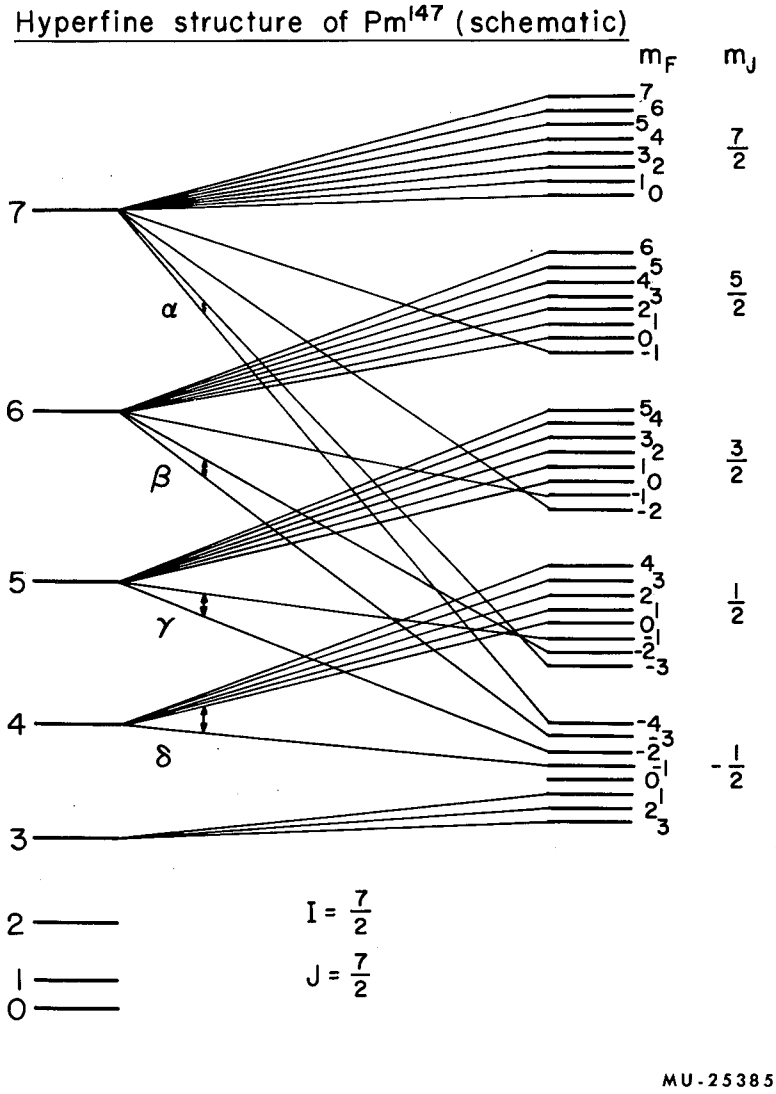

Fig. 3. Hyperfine structure of Pm^{147} (schematic).

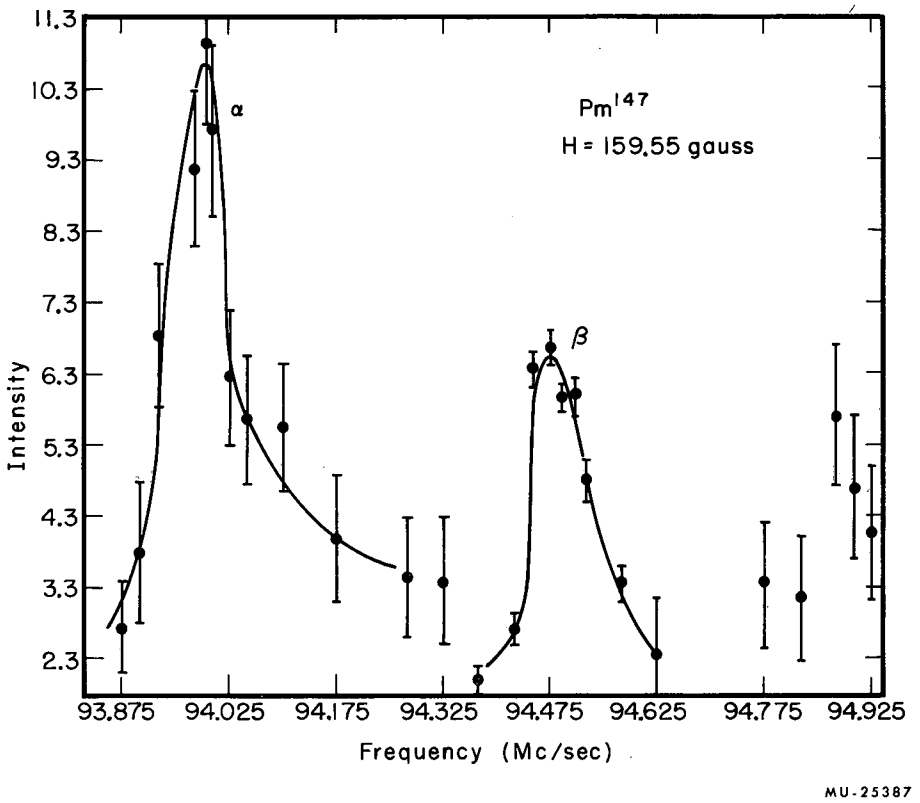

Fig. 4. Transitions in Pm^{147}.

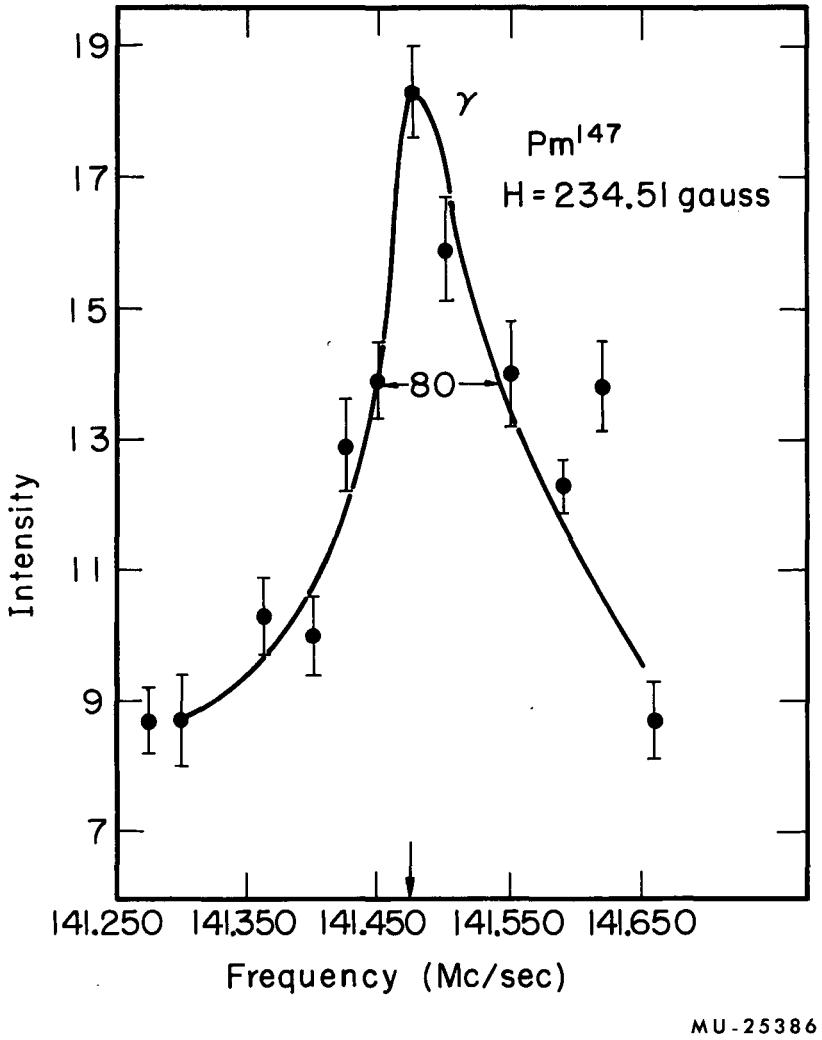

Fig. 5. Resonance in Pm^{147}.

Table I. Summary of observations in Pm^{147}

H (gauss)	Transition	ν(exp) (Mc/sec)	Residuals (Mc/sec)
20.75	α	12.06	+0.009
38.24	α	22.28	+0.035
71.63	α	41.815	+0.006
117.68	α	69.025	+0.008
117.68	β	69.30	-0.009
159.55	β	94.49	-0.018
159.55	γ	95.0	-0.031
159.55	α	93.99	+0.021
238.62	α	141.68	+0.001
238.62	β	142.88	-0.012
234.51	γ	141.475	-0.031
320.0	δ	194.36	+0.057
350.0	δ	213.60	-0.008

$$a = 447(9)\ \text{Mc},$$
$$b = -\ 267(71)\text{Mc}, \tag{28}$$
$$g_J = -\ 0.8283(4).$$

For the 13 observations χ^2 had a value of 1.8 with g_I held constant. The 704 program behaved strangely when g_I was varied either alone or together with any of the other variables. The program was relatively insensitive to different constant values of g_I. It held $g_J - g_I$ constant until values of g_I fifteen times too large were tried. A possible explanation may be that for a system of I = J the matrix elements of I_z and J_z are identical. The term in the nuclear moment is therefore absorbed in the g_J value.

Pm has the configuration $4f^5 6s^2$. This was interpolated from the neighboring elements[5] and verified by measuring the g_J values. If the Hund's Rule ground state is assumed we may use Eqs. (11) and (15) to extract values for the moments

$$|\mu| = 3.2(3)\text{nm},$$
$$|Q| = 1(.3)\text{b}. \tag{29}$$

VI. ELECTRONIC STRUCTURE OF PROMETHIUM

A. Introduction

The deviation of the measured g_J from the Russel-Saunders value of 0.8250 indicates that the spin-orbit effect is not negligible. In what follows, therefore, higher terms will be admixed into the Hund's Rule ground state, the extent of the admixture being estimated through the correction to the g_J value. The new electronic wave function will give a different value for the magnetic field at the nucleus and hence will modify the value of the magnetic moment quoted in the preceding paragraph.

The involved calculation about to be described was undertaken for two additional reasons. First, because as an exercise in perturbation theory it illustrates the power and generality of the technique hinted at in the Introduction. Second, because the group-theoretical methods developed by Racah[42] provide an elegant and beautiful technique for disentangling the complex spectra of f-electron atoms.

Calculations involving f electrons become prohibitively tedious in terms of determinental product functions. The sequence of simplifications that can be introduced has been reviewed.[43] Part of the difficulty stems from there being more than one term with the same values of L and S. These quantum numbers are no longer sufficient. The case of the ^2D's of d^3 is given by Condon and Shortley without specifying the nature of the new quantum numbers.

Group theory enables us to differentiate the set of terms belonging to the same value of L and S by labels for the irreducible representations of the groups R_7 and G_2. These are the analogs of the quantum number L in configurations of two electrons and are denoted by $W = (w_1 w_2 w_3)$ and $U = (u_1 u_2)$. R_7 is the rotation group in seven dimensions and G_2 is a subgroup of R_7. The group-theoretical classification of states is shown in Table II. Here v is a quantum number related to the seniority.

Table II. Group theoretical classification of states for f^5.

v	W	U	SL
5	(110)	(10)	6F
		(11)	6PH
5	(211)	(10)	4F
		(11)	4PH
		(20)	4DGI
		(21)	4DFGHKL
		(30)	4PFGHIKM
3	(111)	(00)	4S
		(10)	4F
		(20)	4DGI

B. Coulomb Interaction

Since the promethium spectrum as observed by Meggers[44] served only to identify it as element 61 and yielded no data on term separations, these energies had to be calculated.[43] The results are listed in Table III. The primes indicate that a linear combination of terms actually has the listed energy. In order to find the correct linear combination corresponding to a particular eigenvalue the matrix of the Coulomb interaction must be set up.

For example, it was known[45] that the principal contribution to the spin-orbit correction is made by the ^4G terms of f^5. There are four such terms. The linear combination of lowest energy lies 51.1 F_2 above the ground state. This number is computed in the following way.

Rather than write the Coulomb energy as an expansion in Slater integrals, Racah showed that it could be written as $\Sigma_k e_k E^k$, where the E^k are linear combinations of the F_k. The e_k are eigenvalues of certain operators, and methods for finding them are given. To reduce the matrix to a single parameter we require ratios of Slater integrals given by Judd,[46]

$$\frac{F_4}{F_2} = 0.138, \qquad \frac{F_6}{F_2} = 0.0151 \ . \tag{30}$$

Then the E^k may be evaluated as

$$\begin{aligned} E^0 &= -18.87\ F_2, & E^2 &= 0.077\ F_2, \\ E^1 &= 14.68\ F_2, & E^3 &= 1.49\ F_2 \ . \end{aligned} \tag{31}$$

Table IV is the matrix of the Coulomb energy within the ^4G terms. The matrix is symmetrical about the diagonal. An identical result appeared in the literature after the calculation had been made.[47] In units of F_2 the matrix may be evaluated as

$$\begin{pmatrix} 63.7 & 8.3 & 23.2 & -6.8 \\ & 86.2 & -2.8 & 26.1 \\ & & 92.3 & -61.1 \\ & & & 132.1 \end{pmatrix} \tag{32}$$

Table III. Term energies for f^5.

Term	Energy (in F_2)
6H	0.0
6F	13.4
4I	48.4
4M	48.7
4F	49.0
4G	51.1
4K	56.6
4L	59.1
6P	62.6
4D	63.0
4H	65.4
4P	71.1
4G'	71.7
4F'	81.9
4I'	84.8
4H'	107.2
4G''	107.4
4K'	116.0
4P'	125.3
4D'	136.2
4H''	143.1
4S	145.5
4F''	147.4
4D''	160.6
4I''	165.9
4F'''	183.8
4G'''	197.6

TABLE IV

	(211)(20)	(211)(21)	(211)(30)	(111)(20)
(211)(20)	$5E_1 - \frac{1040}{7} E_2 + \frac{8}{7} E_3$	$-\frac{16}{7}\sqrt{33\cdot 65}\, E_2 + 5\sqrt{\frac{11\cdot 65}{147}}\, E_3$	$52\sqrt{15}\, E_2 + 4\sqrt{\frac{5}{3}}\, E_3$	$-\frac{12}{\sqrt{7}} E_3$
(211)(21)	$-\frac{16}{7}\sqrt{2145}\, E_2 + \frac{5}{21}\sqrt{2145}\, E_3$	$5E_1 + \frac{1089}{7} E_2 + \frac{11}{21} E_3$	$-16\sqrt{143}\, E_2 + \frac{2}{3}\sqrt{143}\, E_3$	$\frac{\sqrt{33\cdot 65}}{7} E_3$
(211)(30)	$52\sqrt{15}\, E_2 + 4\sqrt{\frac{5}{3}}\, E_3$	$-16\sqrt{143}\, E_2 + \frac{2}{3}\sqrt{143}\, E_3$	$5E_1 + 104\, E_2 + \frac{22}{3} E_3$	$-4\sqrt{105}\, E_3$
(111)(20)	$-\frac{12}{\sqrt{7}} E_3$	$\frac{\sqrt{33\cdot 65}}{7} E_3$	$-4\sqrt{105}\, E_3$	$9 E_1$

It has a lowest eigenvalue of 37.7 F_2. But

$$\left\langle 6H\,(110)\,(11)\;\middle|\;\sum_k e_k E^k\;\middle|\;6H\,(110)\,(11)\right\rangle = -\,9\,E_3 = -\,13.4\,F_2\,. \tag{33}$$

Therefore the lowest eigenvalue lies 51.1 F_2 above the ground state. Corresponding to it there is an eigenfunction

$$\left|{}^4G\right\rangle = 0.484\;\left|\;(211)\,(20)\right\rangle + 0.129\;\left|\;(211)\,(21)\right\rangle - 0.727\;\left|\;(211)\,(30)\right\rangle - 0.471\;\left|\;(111)\,(20)\right\rangle\,. \tag{34}$$

C. The Spin-Orbit Interaction

Using this wave function, we can compute the correction to the g_J value. Matrix elements of the spin-orbit operator $\Lambda = \xi \sum_i \underset{\sim}{s}_i \cdot \underset{\sim}{\ell}_i$ are given by[43]

$$\begin{aligned}(\tau\,LSJM\,|\Lambda|\,\tau'L'S'JM) = n\xi\;&\left\{\frac{3}{2}\,\ell(\ell+1)\,(2\ell+1)\,(2L+1)\right.\\ &\left.(2L'+1)\,(2S+1)(2S'+1)\right\}^{1/2}\\ \times W(JLS'1;SL')\;&\sum_{\overline{\tau}\,\overline{L}\,\overline{S}}(\tau LS\left\{\,|\,\overline{\tau}\,\overline{L}\,\overline{S}\right)(\tau'L'S'\left\{\,|\,\overline{\tau}\,\overline{L}\,\overline{S}\right)\end{aligned} \tag{35}$$

$$\times W(\overline{S}\,S\,\tfrac{1}{2}\,1;\,\tfrac{1}{2}\,S')\;W(\overline{L}\,L\,\ell\,1;\,\ell\,L')\,,$$

where the W's are Racah coefficients related to the 6-j symbol and $(\tau\,L\,S\left\{\,|\,\overline{\tau}\,\overline{L}\,\overline{S}\right)$ are fractional percentage coefficients (fpc). These are merely numbers relating a state of configuration ℓ^n to products of states of the first n-1 electrons with that of the nth electron, e.g.,

$$\psi(\ell^n S\,L\,M_L M_S) = \sum_{\overline{\tau}\,\overline{S}\,\overline{L}}(\ell^n\,\tau\,S\,L\left\{\,|\,\ell^{n-1}\,\overline{\tau}\,\overline{S}\,\overline{L}\right)\sum_{\overline{M}_S\,\overline{M}_L m_s m_\ell}(\overline{S}\,\tfrac{1}{2}SM_S\,|\,\overline{S}\tfrac{1}{2}\overline{M}_S m_S) \tag{36}$$

$$\times(\overline{L}\,\ell\;L\,M_L\,|\,\overline{L}\,\ell\;\overline{M}_L m_\ell)\,\overline{\psi}(\ell^{n-1}\,\overline{\tau}\,\overline{S}\,\overline{L}\,\overline{M}_S\overline{M}_L)\,\phi(\ell m_s m_\ell)\,.$$

By a theorem due to Racah the fpc can be factored into a product of three terms,

$$(f^{n-1}(U'v'S'L')\, f\, S\, L \,|\, \Big\{ f^n\, U\, v\, S\, L) \qquad (37)$$
$$= (U'L'+f \,|\, U\, L)\,(W'U'+f \,|\, WU)\,(f^{n-1}v'S'+f|f^n vS),$$

and each of these is evaluated separately.

The sum in (35) is to be taken over the common parents of ^6H and ^4G. These are the quintets of f^4, excluding ^5S. With $\overline{S} = 2$, $J = 7/2$, $L = 5$, $L' = 4$, $S = 5/2$, $S' = 3/2$, Eq. (35) can be written

$$\left\langle {}^6H_{\frac{7}{2}} \,|\mathbb{A}|\, {}^4G_{\frac{7}{2}} \right\rangle = -\,18\,\xi\sqrt{\frac{77}{5}}\ \sum_{\overline{\psi}}\ (\psi \Big\{ |\,\overline{\psi})\ (\psi' \Big\{ |\,\overline{\psi})\ W(\overline{L}\,531;34), \qquad (38)$$

where the fpc have been abbreviated. They are tabulated in Appendix III. For $|\, {}^4G_{\frac{7}{2}} \,\rangle$ Eq. (34) is to be used. The entire matrix element is found to be $-2.661\ \xi$.

Judd and Lindgren[48] have given the second-order correction to the g_J value as

$$\Delta g = \sum_m \frac{\langle 0|\mathbb{A}|m\rangle\langle m|g|m\rangle\langle m|\mathbb{A}0\rangle}{E_m^2} - \langle 0|g|0\rangle \sum_m \frac{\langle 0|\mathbb{A}|m\rangle\langle m|\mathbb{A}|0\rangle}{E_m^2}, \qquad (39)$$

where 0 refers to the ground state, ^6H, and m to the excited ^4G terms.

Therefore

$$\Delta g = \left(\frac{2.66\ \xi}{51.1\ F_2}\right)^2 1.0023\ \frac{10}{63} = 0.00343\ . \qquad (40)$$

As recommended by the above authors, $\xi = 909\ cm^{-1}$ and $F_2 = 322\ cm^{-1}$ have been inserted. The other linear combinations of ^4G terms contribute in the ratio 1.227:0.1148: 0.0488: 0.0024.[49] Thus the entire contribution of the ^4G's is 0.00389. There is also a smaller negative

contribution from the ^4H's. If to these are added corrections for relativistic and diamagnetic effects the value -0.8275 is obtained. This is in good agreement with the experimental value.

To find the correct wave function let

$$\psi = \sqrt{1-a^2}\,|\,^6H\,\rangle + a\,|\,^4G\,\rangle$$

and demand that this give the correct g_J value. The result is $a = 0.137$. Therefore, $\psi = 0.991\,|\,^6H_{\frac{7}{2}}\rangle + 0.137\,|\,^4G_{\frac{7}{2}}\rangle$, where $^4G_{\frac{7}{2}}$ is given by (34).

D. Magnetic Field at the Nucleus

For purposes of calculating the magnetic field at the promethium nucleus, the brief table of fpc contained in Appendix III will not suffice. This circumstance arises from the existence of matrix elements of the magnetic hyperfine interaction[8] between the ^4G terms whose parents include the triplets of f^4 according to the relations

$$-\sqrt{10}\,(\ell^n\,\alpha SLJ\,||\,(\underset{\wedge}{s}C^2)^1\,||\,\ell^n\alpha' S' L' J) =$$

$$-\sqrt{30}\,(2J+1)\begin{Bmatrix} S & S' & 1 \\ L & L' & 2 \\ J & J & 1 \end{Bmatrix}(s\,||\,s\,||\,s)\,(\ell\,||\,C^2\,||\,\ell) \qquad (43)$$

$$(\ell^n\alpha\,S\,L\,||\,U^{12}\,||\,\ell^n\alpha' S' L')$$

and

$$(\ell^n\alpha SL\,||\,U^{12}\,||\,\ell^n\alpha' S' L') = n\sum_{\overline{\Psi}}(\psi\,\{|\overline{\Psi})\,(\psi'\,\{|\overline{\Psi})$$

$$(-1)^{\overline{L}+\overline{S}+\ell+\frac{1}{2}+S+L+3}\times\sqrt{(2S+1)\,(2S'+1)\,(2L+1)(2L'+1)}\begin{Bmatrix} s & S & \overline{S} \\ S' & s & 1 \end{Bmatrix}\begin{Bmatrix} \ell & L & \overline{L} \\ L' & \ell & 2 \end{Bmatrix}, \qquad (44)$$

where a 9-j symbol appears in (43) and U^{12} is a double-tensor operator. Such a summation would be extremely difficult. Fortunately, it can be simplified considerably by a theorem due to Judd,[50] who showed that reduced matrix elements of double tensors for the configuration f^5 are proportional to reduced matrix elements of single tensors for the configuration f^4. A correspondence is established between terms according to the labels W and U. In our case this correspondence is as follows.

$$\begin{aligned}
f^5\ {}^6H(110)\ (111) &\longleftrightarrow f^4\ {}^3H(110)\ (111)\\
{}^4G(211)\ (20) &\longleftrightarrow {}^3G(211)\ (201)\\
{}^4G(211)\ (21) &\longleftrightarrow {}^3G(211)\ (21)\\
{}^4G(211)\ (30) &\longleftrightarrow {}^3G(211)\ (30)\\
{}^4G(111)\ (20) &\longleftrightarrow {}^5G(111)\ (20)
\end{aligned} \tag{45}$$

We may therefore write

$$(f^5\ WUSL||U^{12}||f^5W'U'S'L') = a\ (f^4WUSL||U^2||f^4W'U'S'L') \tag{46}$$

and use

$$(f^n a\ SL||U^2||f^n a'S'L') = n\ \delta(SS')\ \sum_{\overline{\Psi}} (\psi\{|\overline{\Psi})\ (\psi'\{|\overline{\Psi})$$

$$(-1)^{\overline{L}+3+L+2}\sqrt{(2L+1)(2L'+1)}\begin{Bmatrix} L & 2 & L' \\ 3 & \overline{L} & 3 \end{Bmatrix}. \tag{47}$$

The simplification consists in that the sum is now over the doublets and quartets of f^3. Judd gives an explicit formula for evaluating the proportionality constant a. It was checked for the (^6H) (^4G) matrix

elements by using (44) and found to have the value $\sqrt{\frac{5}{2}}$. The fpc appearing in (47) are tabulated in Appendix IV. They were checked by using the relation

$$(f^4\ a\ SL\ ||\ U^1\ ||\ f^4 a\ SL) = \sqrt{\frac{L(L+1)\ (2L+1)}{\ell(\ell+1)\ (2\ell+1)}} \tag{48}$$

$$= 4 \sum_{\overline{\Psi}} (\psi \{|\overline{\Psi}) (\psi \{|\overline{\Psi}) (-1)^{\overline{L}+3+L+1} (2L+1) \begin{Bmatrix} L & 1 & L \\ 3 & \overline{L} & 3 \end{Bmatrix} .$$

With the help of the tables in Appendix IV the following matrix of U^2 was constructed.

	^3H	$^3G(20)$	$^3G(21)$	$^3G(30)$	$^5G(20)$
^3H		$\frac{2}{7}\sqrt{\frac{3}{5}}$	$\frac{2^2}{5\cdot 7}\sqrt{\frac{11\cdot 13}{3}}$	$\frac{2}{3\cdot 5}\sqrt{3}$	
$^3G(20)$		$\frac{1}{2\cdot 7^2}\sqrt{3\cdot 11}$	$\frac{2\cdot 11}{7^2}\sqrt{\frac{13}{5}}$	$\sqrt{\frac{5}{11}}$	
$^3G(21)$			$-\frac{113}{2\cdot 5\cdot 7^2}\sqrt{\frac{11}{3}}$	$\frac{2^3}{3\cdot 5\cdot 11}\sqrt{\frac{13}{3}}$	
$^3G(30)$				$\frac{17}{5}\sqrt{\frac{1}{3\cdot 11}}$	
$^5G(20)$					$\frac{1}{2\cdot 7}\sqrt{\frac{3}{11}}$

This is modified to the matrix of U^{12} by introducing the proportionality constant and the easily evaluated first diagonal matrix element.

$$
\begin{array}{c}
\\
{}^6H \\
{}^4G(20) \\
{}^4G(21) \\
{}^4G(30) \\
{}^4G(20)
\end{array}
\begin{array}{c}
\begin{array}{ccccc}
{}^6H & {}^4G(20) & {}^4G(21) & {}^4G(30) & {}^4G(20)
\end{array} \\
\left(\begin{array}{ccccc}
-\frac{1}{3}\sqrt{\frac{11\cdot 13}{2\cdot 5}} & \frac{2^2}{7}\sqrt{2} & \frac{2}{7}\sqrt{\frac{2\cdot 11\cdot 13}{3\cdot 5}} & \sqrt{\frac{2}{3\cdot 5}} & \\
 & \frac{1}{2\cdot 7^2}\sqrt{\frac{3\cdot 5\cdot 11}{2}} & \frac{2\cdot 11}{7^2}\sqrt{\frac{13}{2}} & 5\sqrt{\frac{1}{2\cdot 11}} & \\
 & -\frac{113}{2\cdot 7^2}\sqrt{\frac{11}{2\cdot 3\cdot 5}} & \frac{2^2}{3\cdot 11}\sqrt{\frac{2\cdot 13}{3\cdot 5}} & & \\
 & & & 17\sqrt{\frac{1}{2\cdot 5\cdot 3\cdot 11}} & \\
 & & & & \frac{1}{2\cdot 7}\sqrt{\frac{3\cdot 5}{2\cdot 11}}
\end{array}\right)
\end{array}
$$

The next step is to use (43) to construct the matrix of $(\underset{\sim}{s}\,\underset{\sim}{C}^2)^1$. Appendix V contains the relevant 9-j symbols. We have

$$
\begin{array}{c}
\\
{}^6H \\
{}^4G(20) \\
{}^4G(21) \\
{}^4G(30) \\
{}^4G(20)
\end{array}
\begin{array}{c}
\begin{array}{ccccc}
{}^6H & {}^4G(20) & {}^4G(21) & {}^4G(30) & {}^4G(20)
\end{array} \\
\left(\begin{array}{ccccc}
-\frac{2\cdot 13\cdot 19}{3^2\cdot 5^2}\sqrt{\frac{2}{7}} & \frac{2^6\cdot 11}{3\cdot 5\cdot 7}\sqrt{\frac{1}{3\cdot 5}} & \frac{2^5\cdot 11}{3^2\cdot 5^2\cdot 7}\sqrt{11\cdot 13} & \frac{2^4\cdot 11}{3^2\cdot 5^2} & \\
 & \frac{2\cdot 11\cdot 17}{3^2\cdot 5\cdot 7^2}\sqrt{\frac{2}{7}} & \frac{2^4\cdot 11\cdot 17}{3^2\cdot 5\cdot 7^2}\sqrt{\frac{11\cdot 13}{2\cdot 3\cdot 5\cdot 7}} & \frac{2^3\cdot 17}{3^2}\sqrt{\frac{1}{2\cdot 3\cdot 5\cdot 7}} & \\
 & & -\frac{2\cdot 11\cdot 17\cdot 113}{3^3\cdot 5^2\cdot 7^2}\sqrt{\frac{2}{7}} & \frac{2^5\cdot 17}{3^4\cdot 5^2}\sqrt{\frac{2\cdot 13}{7\cdot 11}} & \\
 & & & \frac{2^2\cdot 17^2}{3^3\cdot 5^2}\sqrt{\frac{2}{7}} & \\
 & & & & \frac{2\cdot 17}{3^2\cdot 5\cdot 7}\sqrt{\frac{2}{7}}
\end{array}\right)
\end{array}
$$

Only the operator $\underset{\sim}{L}$ remains to be evaluated. Its matrix elements are given by

$$(aSLJ||L||a'S'L'J) = \sqrt{\ell(\ell+1)(2\ell+1)}\,(aSLJ||U^{(1)}||a'S'J)$$

$$= \sqrt{\ell(\ell+1)(2\ell+1)}\begin{Bmatrix} J & 1 & J \\ L' & S & L \end{Bmatrix}\delta(S,S')\,\delta(a,a')\,\delta(L,L')$$

$$(-1)^{L+S+J+1}\sqrt{\frac{L(L+1)2L+1}{\ell(\ell+1)(2\ell+1)}} \qquad (49)$$

$$= \begin{Bmatrix} J & 1 & J \\ L' & S & L \end{Bmatrix}(2J+1)\sqrt{L(L+1)(2L+1)}.$$

It is clearly diagonal, and when added to the previous matrix gives

	^6H	$^4G(20)$	$^4G(21)$	$^4G(30)$	$^4G(20)$
^6H	$\frac{2\cdot 37}{3}$	$-\frac{2\cdot 13\cdot 19}{3^2\cdot 5^2}$	$\frac{2^6\cdot 11}{3\cdot 5\cdot 7}\sqrt{\frac{1}{3\cdot 5}}$	$\frac{2^5\cdot 11}{3^2\cdot 5^2\cdot 7}\sqrt{11\cdot 13}$	$\frac{2^4\cdot 11}{3^2\cdot 5^2}$
$^4G(20)$	$\times\sqrt{\frac{2}{7}}$	$(\frac{2^6}{3}+\frac{2\cdot 11\cdot 17}{3^2\cdot 5\cdot 7^2})\sqrt{\frac{2}{7}}$	$\frac{2^4\cdot 11\cdot 17}{3^2\cdot 5\cdot 7}\sqrt{\frac{11\cdot 13}{2\cdot 3\cdot 5\cdot 7}}$	$\frac{2^3\cdot 17}{3^2}\sqrt{\frac{1}{2\cdot 3\cdot 5\cdot 7}}$	
$^4G(21)$			$(\frac{2^6}{3}-\frac{2\cdot 11\cdot 17\cdot 113}{3^3\cdot 5^2\cdot 7^2})\sqrt{\frac{2}{7}}$	$\frac{2^5\cdot 17}{3^4\cdot 5^2}\sqrt{\frac{2\cdot 13}{7\cdot 11}}$	
$^4G(3)$				$(\frac{2^6}{3}+\frac{2^2\cdot 17^2}{3^3\cdot 5^2})\sqrt{\frac{2}{7}}$	
$^4G(20)$					$(\frac{2^6}{3}+\frac{2\cdot 17}{3^2\cdot 5\cdot 7})$
					$\times\sqrt{\frac{2}{7}}$

In numbers, we have

	^6H	$^4G(20)$	$^4G(21)$	$^4G(30)$	$^4G(20)$
^6H	12.02	1.73	2.65	0.782	
$^4G(20)$		11.49	7.96	1.04	
$^4G(21)$			10.71	0.16	
$^4G(30)$				11.63	
$^4G(20)$					11.45

The reduced matrix element of the hyperfine interaction is then

$$(0.991)^2(12.02) + 2(0.137)(0.991)\{(0.484)(0.173) + (0.129)(2.65) - 0.727(0.782)\} + (+.137)^2\{0.484[11.49(0.484) + 2(0.129)(7.96) - 2(0.727)(1.04)] + 0.129[0.129(10.71) + 2(-0.727)(0.16)] + (0.727)^2(11.63) + (0.471)^2(11.45)\}$$

$$= 12.19,$$

where we have used the corrected wave function. On the other hand, the matrix element of the same operator for the pure Hund's Rule state is 12.02. The nuclear moment should therefore be reduced by about 2%.

VII. HOLMIUM-161

A. Introduction

The incentive for measuring the nuclear spin of Ho^{161} was twofold. First, to use the cyclotron to produce otherwise inaccessible radioactive isotopes. This involved ascertaining that a high enough specific activity could be reached with the available facilities. Second, to establish the J value of the lowest level of the ^4I term arising from the configuration $4f^{11}6s^2$. The value $g_J = 1.19516(10)$ measured in conjunction with the spin of Ho^{166} [51,52] suggested Russel-Saunders coupling to a J of $\frac{15}{2}$. While the work was in progress a more definite assignment was made based on stable Ho^{165}. The half life of Ho^{161} was known to be 2.5 h.[53]

B. Beam Production

Natural dysprosium, in the form of pellets, was bombarded in the 60-inch Crocker cyclotron. Figure 6 shows the water-cooled "jumbo" target holder and the ten-hole plate in which the pellets are placed. A 1-mil aluminum foil covering the ten-hole plate prevents the pellets from falling out. A variety of bombardment conditions was tried. Protons at 12 MeV and 30 μA seemed to produce the purest 2.5-h activity at a sufficient level. A decay curve, Fig. 7, indicates that during the experiment Ho^{161} was the primary component in the beam. It also shows the presence of a 5-h component, presumably Ho^{160m},[54] present according to the reaction

$$_{66}Dy^{161} + p \longrightarrow {}_{67}Ho^{160m} + 2n .$$

Attempts to minimize this component through the d, 2n reaction with deuterons of varied energy were unsuccessful. In addition, terbium was used as a target material with α particles as projectiles. A complicated spectrum was then obtained, since both components were in the beam.

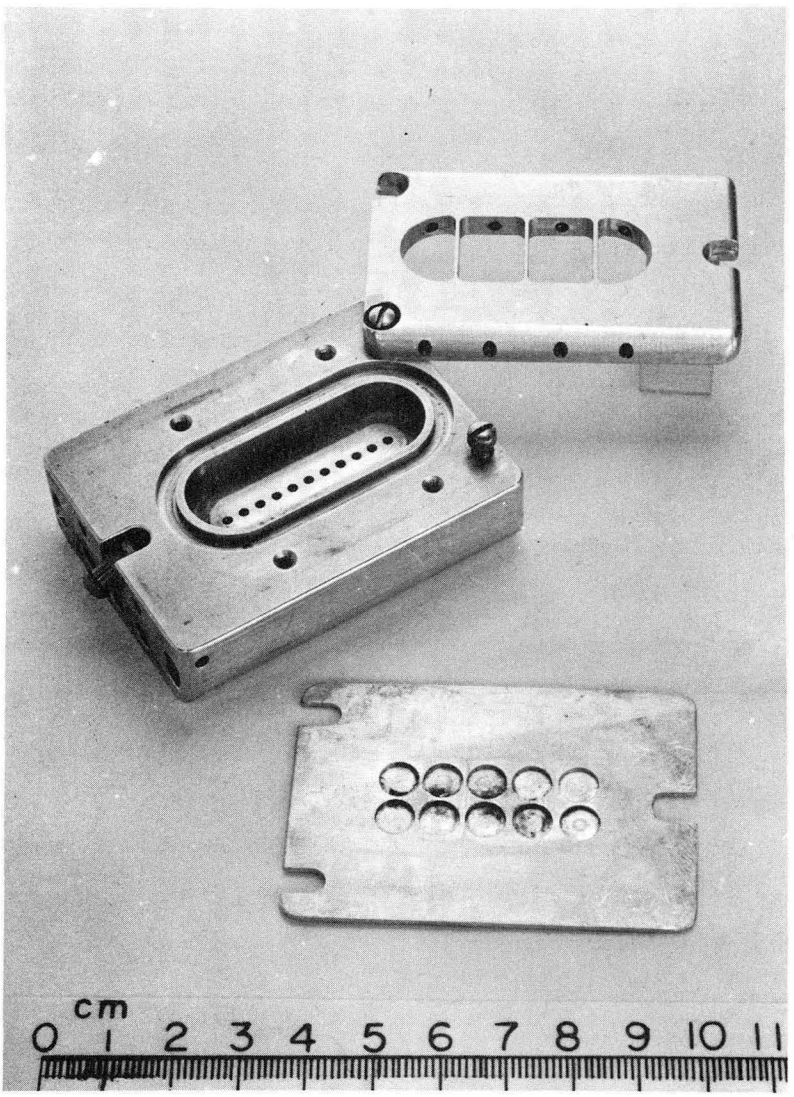

ZN-3122

Fig. 6. Jumbo target and ten-hole plate.

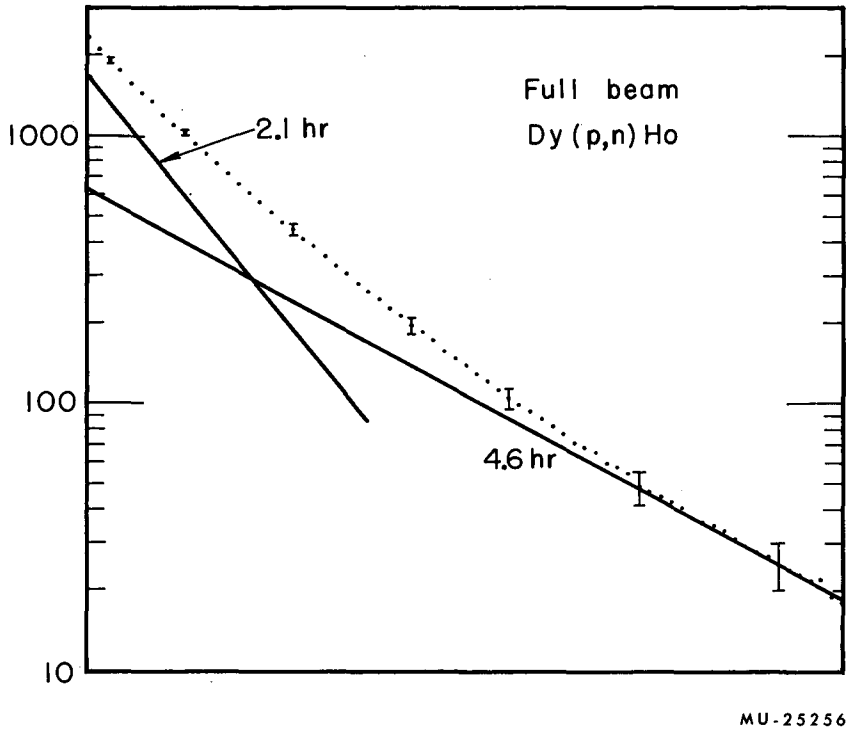

Fig. 7. Decay of the full beam.

Even with protons the low specific activity resulted in serious arcing problems in the oven. Two new ovens were designed to conserve material. They are shown in Fig. 8. To prevent the slit and holes from clogging the tungsten filament was mounted in front of the oven. Little success attended all these efforts. Only careful outgassing before a run and meticulous cleaning of the oven loader finally reduced the arcing problem.

In the early stages of the work the activity was observed in x-ray counters, the x rays accompanying the electron-capture mode of decay. Subsequently, it proved both feasible and convenient to count the Auger electrons that are also emitted by the excited atom.

C. Results

Figures 9 and 10 and Table V show the results of two field searches at 5.567 and 8.246 gauss respectively. Five of the eight flop-in transitions were observed at the lower field and three at the higher field. They all correspond to a spin of $\frac{7}{2}$ with $J = \frac{15}{2}$. The initial search at 2 Mc of potassium yielded curves consistent with this assignment but more poorly resolved. Interpretation of the spin measurement is reserved for the discussion of nuclear structure.

D. Interpretation of the J Value

The measured g_J value is close to the Russel-Saunders value, -1.2, for 11 f electrons coupling to a $^4I_{15/2}$ ground state. However, experiments on Ho^{166} did not confirm the J value and the possibility existed that the configuration was $4f^{10}5d$. Cabezas[55] showed that Russel-Saunders coupling between shells gives rise to a ground term ^6L with the following J and g_J values:

$$^6L_{21/2} \qquad g_J = -1.2381,$$

$$^6L_{19/2} \qquad g_J = -1.1829;$$

An excited $^6K_{19/2}$ level with $g_J = -1.2631$ also would exist.

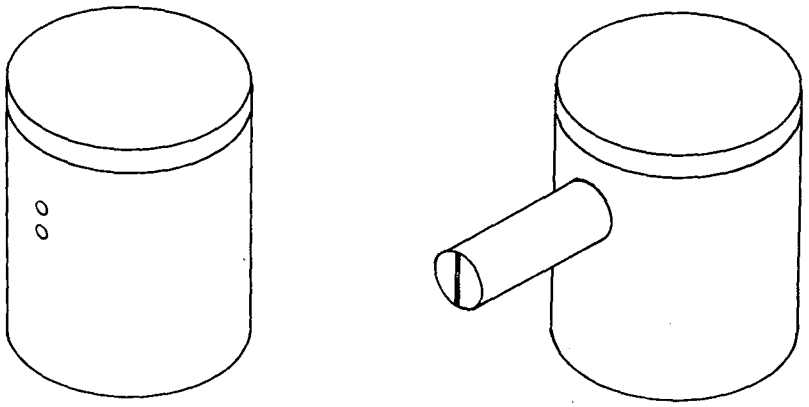

Fig. 8. Collimated Ovens for Holmium

MU-26750

Fig. 8. Collimated ovens for holmium.

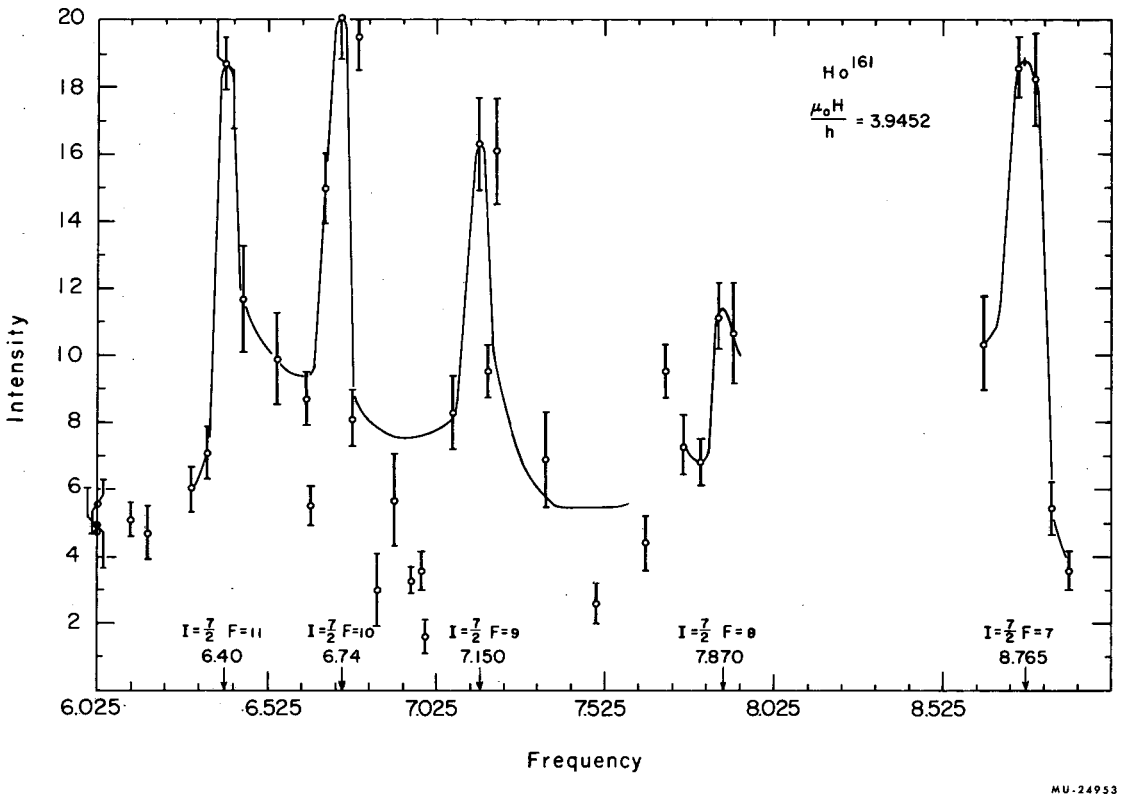

Fig. 9. Observations in Ho^{161}.

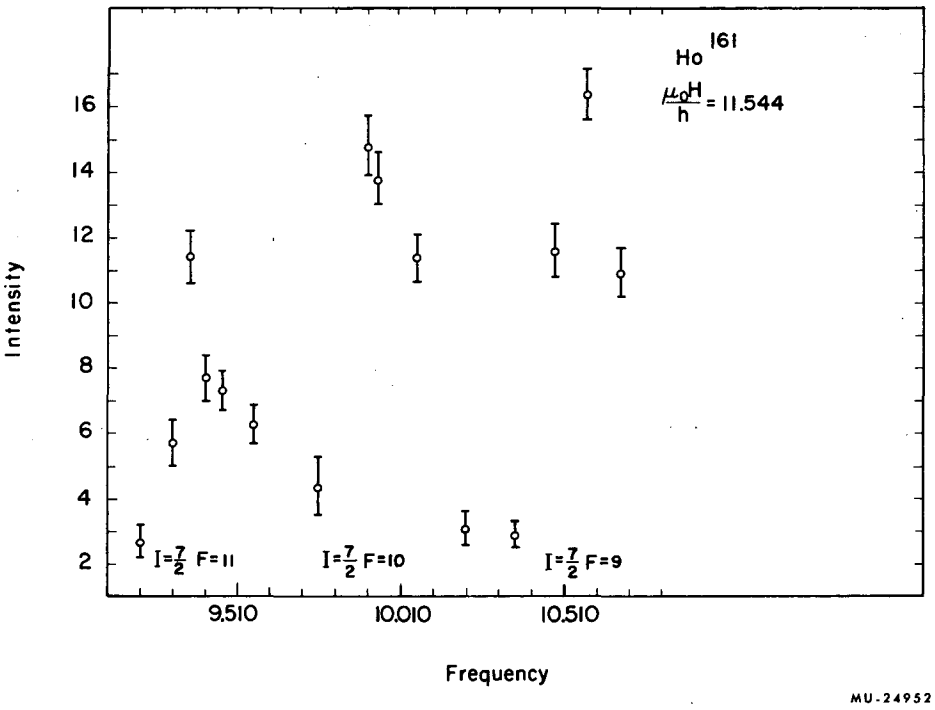

Fig. 10. Observed transitions in Ho^{161}.

Table V. Summary of observations in Ho^{161}.

$\frac{\mu_0 H}{h}$ (Mc)	F state	Observed frequency (Mc)	Predicted frequency (Mc)
7.7917	11	6.40(7)	6.352
7.7917	10	6.74(9)	6.691
7.7917	9	7.15(8)	7.143
7.7917	8	7.87(10)	7.760
7.7917	7	8.765(120)	8.800
11.544	11	9.315(50)	9.411
11.544	10	9.910	9.913
11.544	9	10.580	10.582

Since there is no other term with $J = 21/2$, the entire deviation of g_J for $^6L_{21/2}$ from the measured value would have to be explained by relativistic and diamagnetic effects. Alternatively, the ground term could be a linear combination of $^6L_{19/2}$ and $^6K_{19/2}$, the latter admixed through the spin-orbit interaction. The coefficients could be adjusted to give the measured g_J. Plausible as this may seem, it remains to be explained why $^6L_{19/2}$ and not $^6L_{21/2}$ should be the ground level.

Even with J established as $15/2$, the $f^{10}d$ configuration cannot be ruled out because one need not assume R-S coupling between shells. R-S coupling may exist within each shell, but the shells may be j-j coupled to one another, e.g.,

$$\left({}^5I_8 \quad {}^2D_{3/2} \right)_{\frac{15}{2}} .$$

In addition to the fact that this coupling gives rise to a g_J that is far from experiment (for $J = 15/2$), it may also be ruled out on plausibility grounds. Two other configurations that are known to contain a d electron, gadolinum and terbium, definitely exhibit R-S coupling between shells.

In the light of these considerations the J of $15/2$ measured in this experiment, together with the previously measured $g_J = -1.1956$, lend strong support to the configuration assignment $4f^{11}$.

VIII. ERBIUM-165

A. Introduction

Cabezas measured the spins of Er^{169} and Er^{171} in this Laboratory.[56] The values $J = 6$, $g_J = -1.164(5)$ were consistent with his data. Smith and Spaulding[57] independently determined the J state by measuring g_F for the stable Er^{167}. Its spin was known to be 7/2 from paramagnetic resonance.[58] They then found g_J by observing flop-in transitions in Er^{166}.

The integral spin implies that the observable transitions must be of the multiple-quantum type. These were in fact observed.[55] Increasing the rf power greatly enhances the resonance intensity, since the transition probability for an n-quantum transition goes as the 2nth power of the rf field. This enhancement has been observed in work on the hfs of Er^{171}.[59] A triple quantum transition appears as a satellite of the main peak in the K^{39} calibration and can be readily observed on our apparatus.

B. Beam Production

One-hundred-percent-abundant Ho^{165} was bombarded on the 60-inch cyclotron to produce Er^{165} according to the reaction

$$_{67}Ho^{165} + p \longrightarrow {}_{68}Er^{165} + n .$$

A decay of the direct beam, Fig. 11, shows a pure 9.8-hour product. This is consistent with the 9.9(1)-h half life that had been assigned previously.[60] The holmium was in the form of discs or pellets and the beam was produced by boiling directly out of the holmium. A high specific activity minimized arcing problems.

C. Results

A schematic diagram of the hfs for a system $J = 6$, $I = \frac{5}{2}$ is shown in Fig. 12. Six flop-in transitions are observable. Of these, four were observed at 2 Mc of potassium and again at 5 Mc. They are shown in Figs. 13 and 14. The linear dependence of the resonant frequency

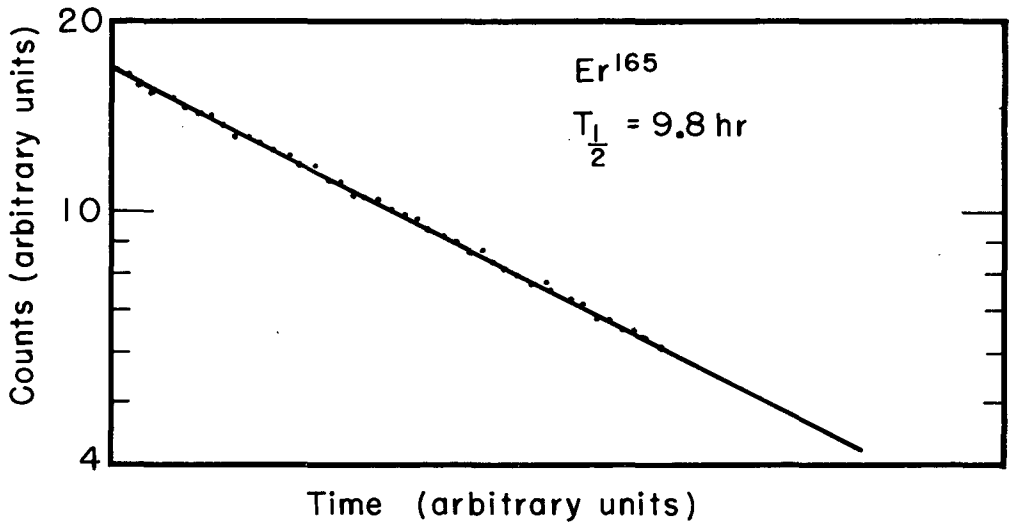

Fig. 11. Decay of Er^{165} direct beam.

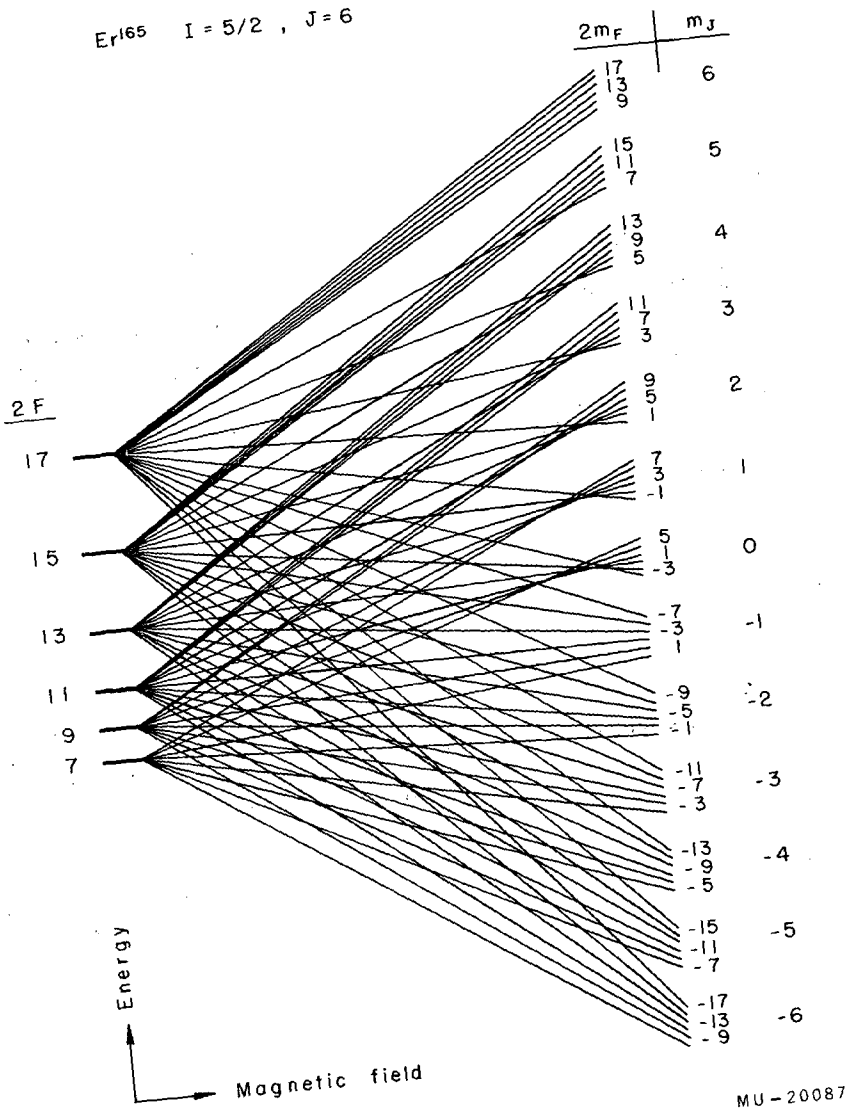

Fig. 12. Hfs schematic of Er^{165}

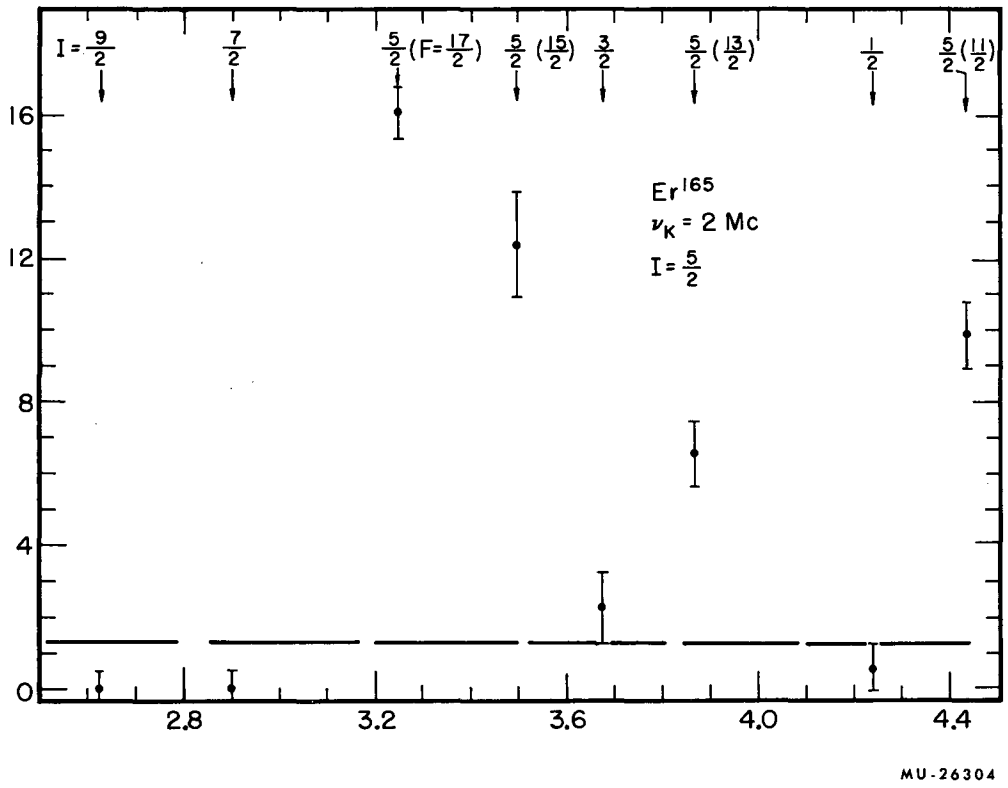

Fig. 13. Four transitions observed in Er^{165}.

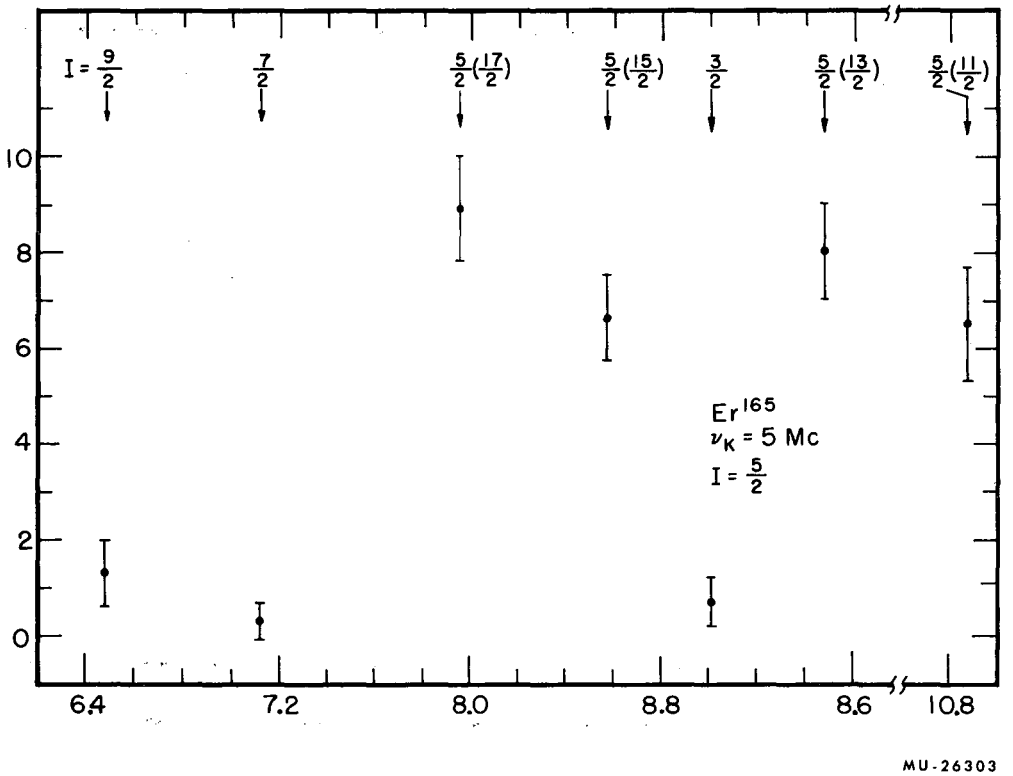

Fig. 14. The four Er^{165} transitions at higher field.

on field, in accordance with (21), serves to confirm the g_J value. The latter, in turn, together with the half life and method of production conclusively identify the isotope as Er^{165}.

IX. PRASEODYMIUM-143

A. Introduction

Praseodymium has only one stable isotope, of mass 141. The lowest terms of Pr II were found to belong to the configuration f^3s.[61] It was then suggested[62] that the ground state of PrI was probably f^3s^2, $^4I_{9/2}$. Hin Lew confirmed this level assignment and established the g_J value as -0.731(2) in his work on the hfs and nuclear moments of Pr^{141}.[63] The hfs constants and moments of Pr^{142} (19 h) have also been measured.[64]

Pr^{143} was discovered almost simultaneously by three groups.[65] It was subsequently identified as a fission product.[66] The two most recent half-life determinations report 13.76(5) and 13.59(4) days.[67,68] There is a more serious disagreement in the prediction of the ground-state spin. Martin et al. argue in favor of a d $\frac{5}{2}$ assignment,[69] since the β decay from the h $\frac{9}{2}$ level of Ce^{143} to the ground state of Pr^{143} is not observed. A $\Delta\ell$ of 3 would make this transition "ℓ-forbidden." Kondaiah predicts a spin of $\frac{7}{2}$ on the basis of x-ray multipolarities, ft values, and the spin-orbit coupling model.[70]

B. Beam Production

Production of Pr^{143} proceeds through a double neutron capture on Pr^{141}. Two high successive cross sections make this method feasible. Stable Pr was bombarded at the government plant in Arco, Idaho for 3 weeks at a flux of 5×10^{14} neutrons/cm^2-sec. The decay curve, Fig. 15, shows the method's success.

Line-up problems hampered the early runs. The oven slit shifted out of the field of view as the temperature was raised. The concomitant decrease in beam intensity was attributed to interaction of the Pr with the tantalum oven. An optical analysis of the tantalum was made to be sure it was free of impurities.

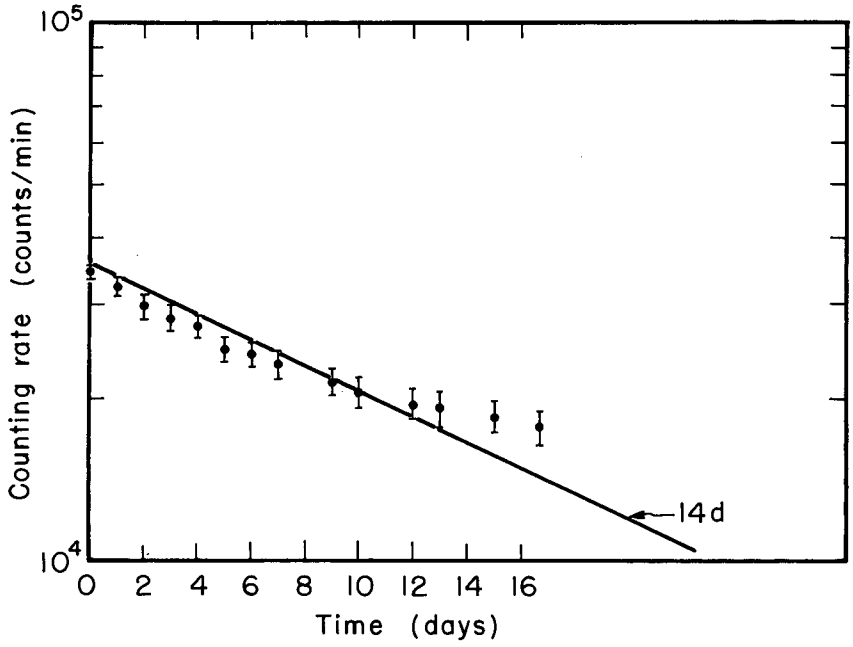

Fig. 15. Decay curve of Pr^{143}.

C. Results

Figure 16 shows that five flop-in transitions are observable. Three were seen at 2 Mc of potassium, two at 4 Mc and one traced out at 8 Mc. They all correspond to a spin of 7/2. The data are illustrated in Figs. 17, 18 and 19. We thus encounter a case similar to the anomalous decay of Nd^{147}, in which a transition that should be at most first-forbidden is totally absent.

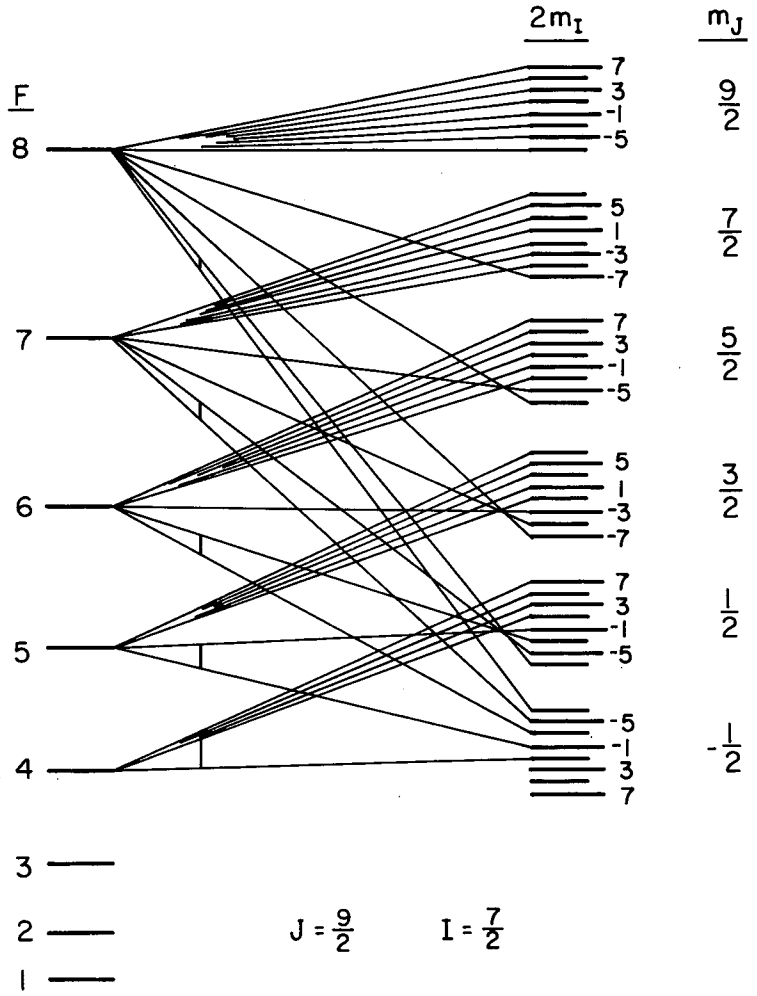

Fig. 16. Hfs schematic of Pr^{143}.

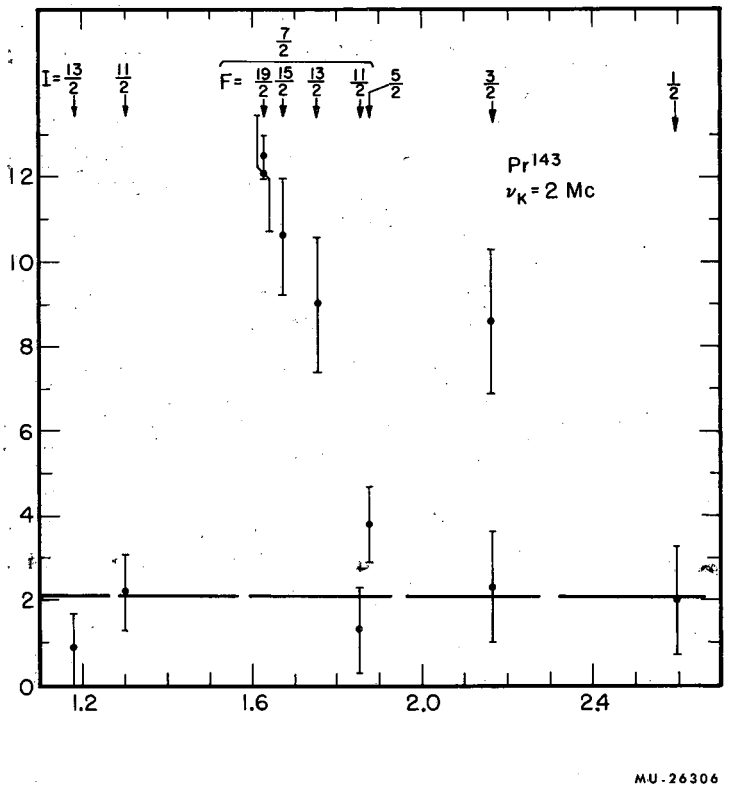

Fig. 17. Resonances observed in Pr^{143}.

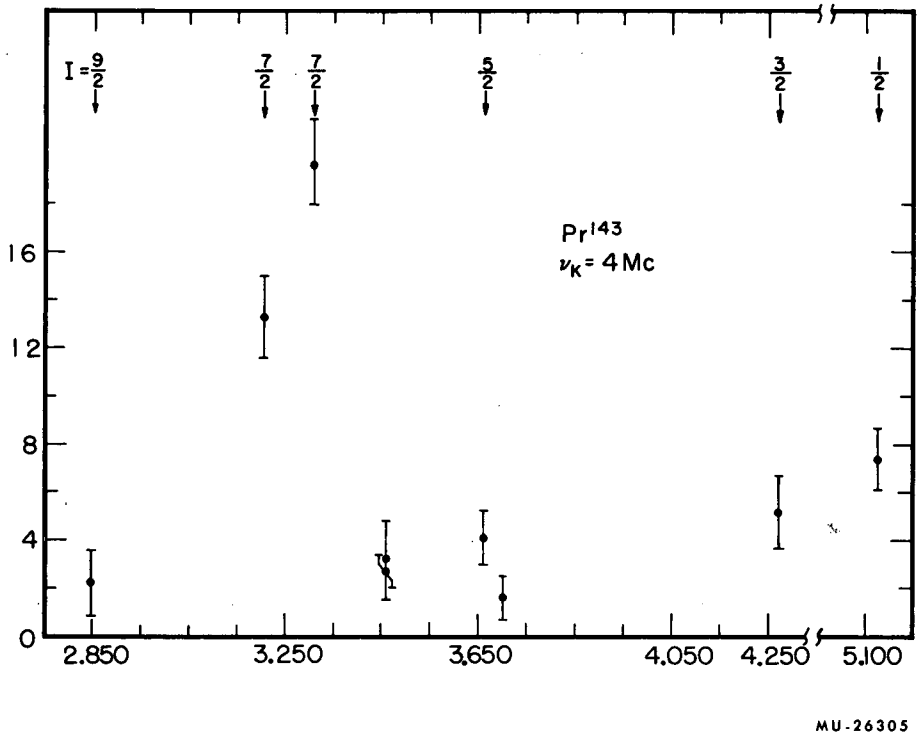

Fig. 18. Two transitions in Pr^{143}.

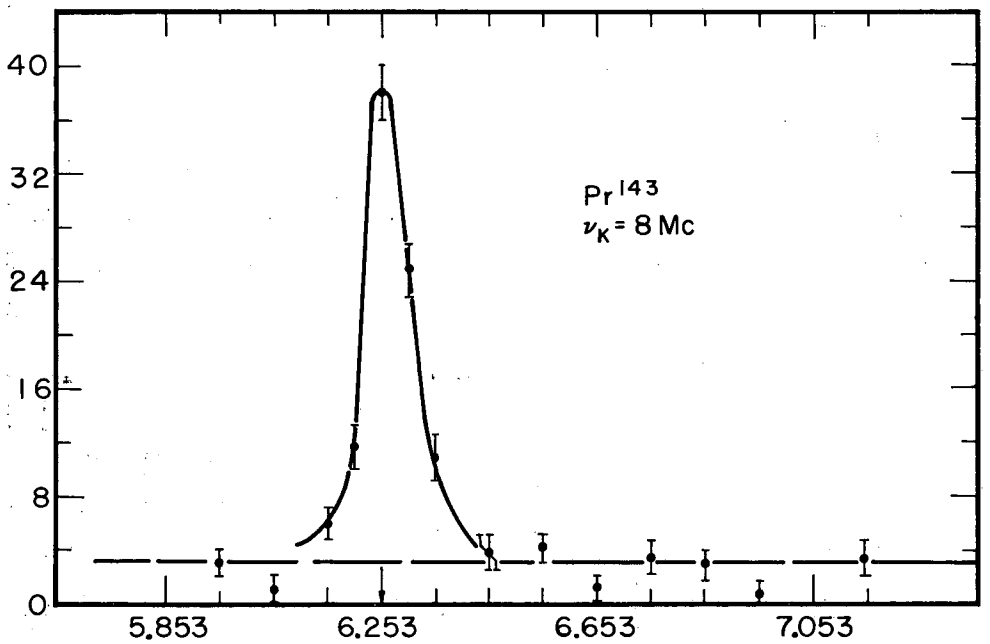

Fig. 19. An α transition in Pr^{143}.

X. NEODYMIUM-149

A. Introduction

The half life and β spectrum of the neodymium isotope of mass number 149 have been measured and the half life found to be 1.8 hours.[71] Schuurmanns suggested the f^4s^2 configuration and the Hund's Rule ground term $^5I_4$.[62] By a method similar to the one used for erbium, Smith and Spalding[56] established the ground-level assignment and measured a g_J of-0.6032(1). Their method, which depends on the even-Z character of an element, implies that J is integral and the transitions therefore of the multiple-quantum variety.

B. Beam Production

The short half life and abundance of longer-lived reaction products necessitate a short neutron-irradiation period of the natural Nd. Bombardments of 2 and 4 hours were tried. Figure 20 shows that with a 4-h irradiation the counting rates of Nd^{149} and longer-lived components were approximately equal at the inception of an experiment. The longer-lived products are Pm^{149}, to which the neodymium decays, and Pm^{151}. Indeed, the same reaction, except for longer periods, is used to produce these isotopes. The beam characteristics were further complicated by two apparently different distillation temperatures. One component distilled at 80 watts of oven power and the other at 160 watts. It was believed that this character was due to the presence of lower oxides or suboxides of neodymium.[72] As mentioned earlier, it was discovered that the oven position relaxed as the temperature was raised. At a power close to 80 watts the oven slit shifted out of the narrow field of view. A power of 160 watts boiled out atoms in such profusion that a beam could be detected. This beam soon died.

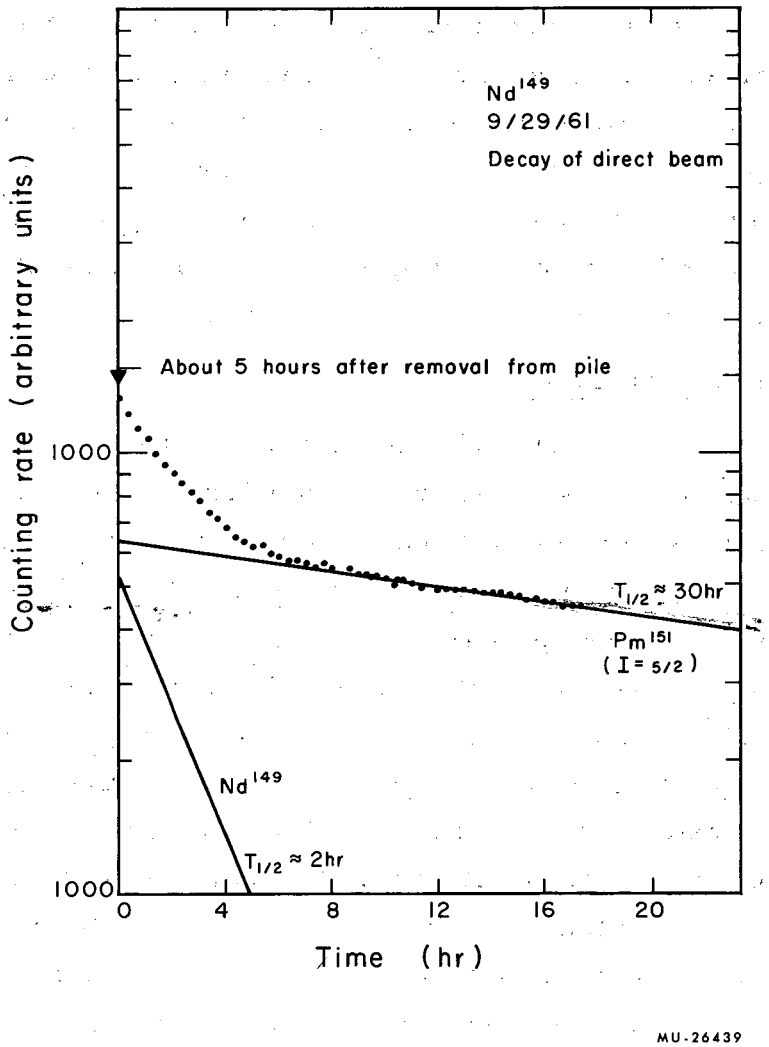

Fig. 20. Result of natural Nd irradiation.

C. Results

Once this tendency was discovered and compensated for, by realigning the oven slit, resonances were easily observed. A schematic diagram of the hfs for a system of $J = 4$, $I = \frac{5}{2}$ is shown in Fig. 21. At 2 Mc of potassium, transitions were observed in the $J = 5$ state as well, and at 4 Mc even the $J = 6$ state was observed in the beam. This is consistent with earlier findings.[56] The results are shown in Figs. 22 and 23 and tabulated in Table VI.

It was important to establish that the resonances had a 1.8-h half life, since Nd^{147} also has a spin of 5/2. Fortunately, the latter has a much longer half life and is easily distinguished. A decay of two resonance buttons is shown in Fig. 24. The tail of the curve is presumably due to machine background, the Pm isotopes.

D. Implications for the Fine-Structure Separations

Although the intensities of the transitions in the different J states were not investigated carefully, they appeared to be approximately equal. The measured fine-structure separations[73] and g_J values are listed in Table VII. If the oven temperature is assumed to be 2000°C, the relative population (in %) of each level may be calculated. These values are also entered in the table. The equal intensities may occur because the higher g_J values associated with states of larger J give rise to the larger deflections that are necessary to clear the stop wire.

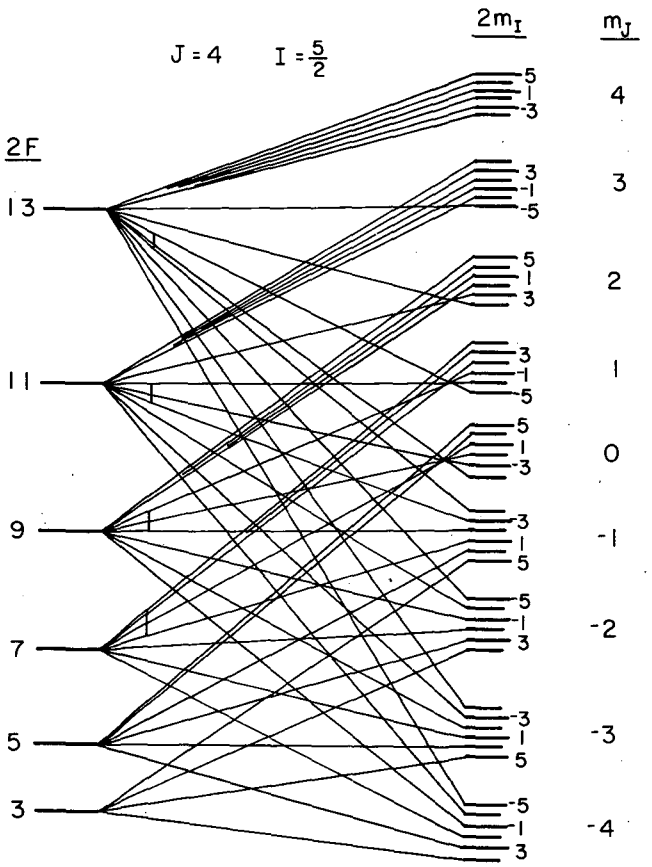

Fig. 21. Hfs schematic of Nd^{149}.

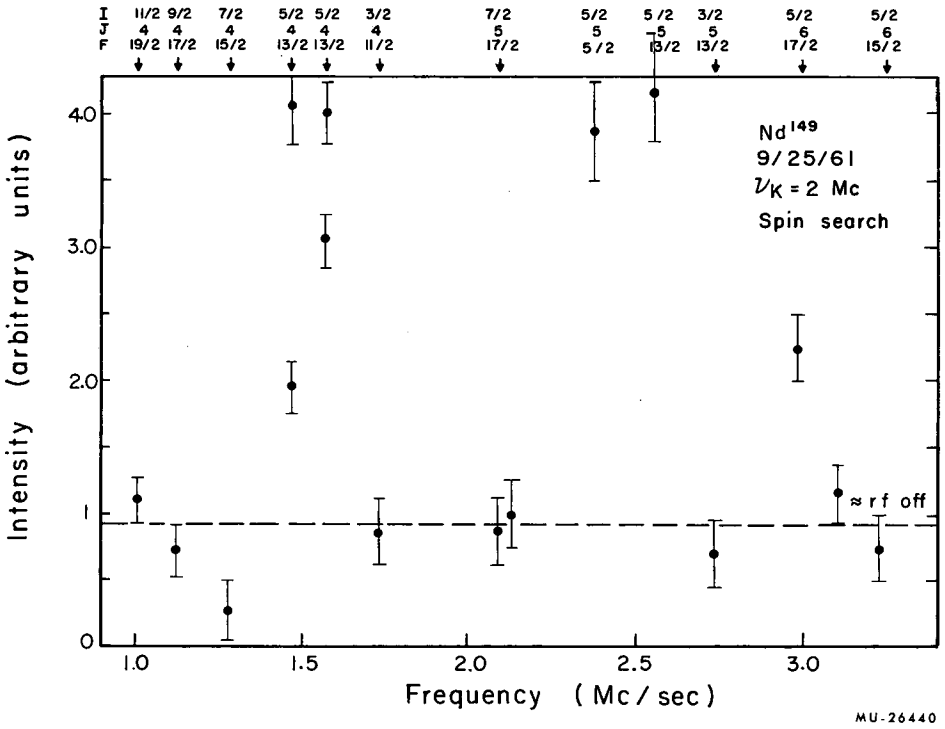

Fig. 22. Resonances observed in Nd^{149}.

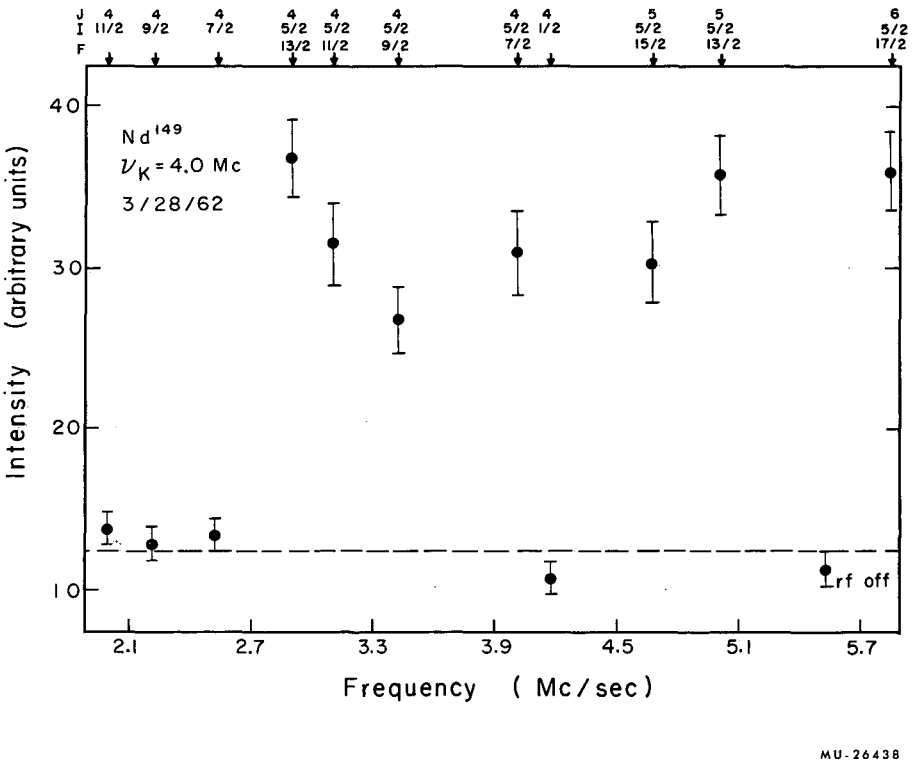

Fig. 23. Observed transitions in Nd^{149}.

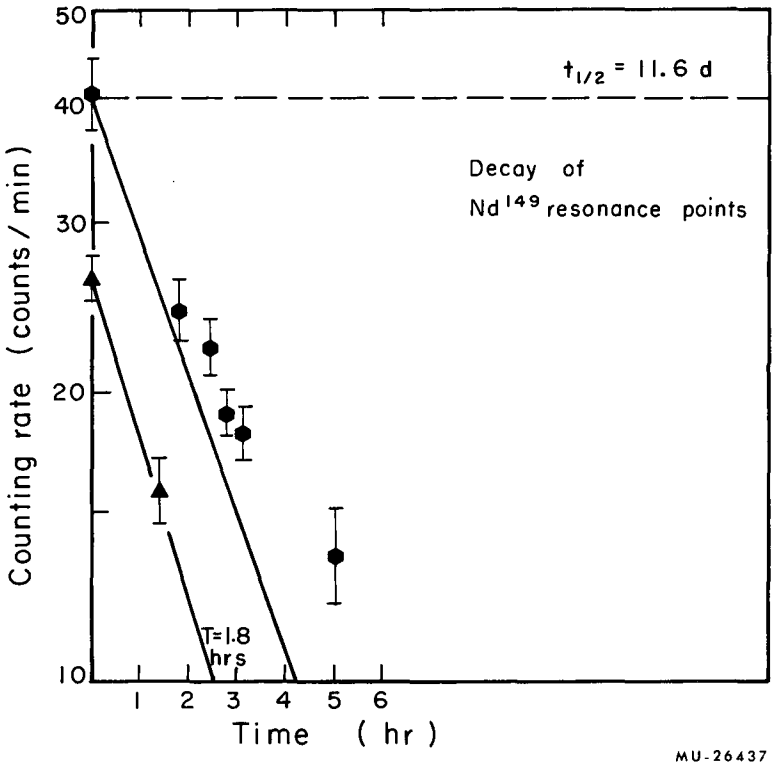

Fig. 24. Decay of Nd^{149} resonance buttons.

Table VI. Observations in Nd^{149} ($I = \frac{5}{2}$).

$\frac{\mu_0 H}{h}$	J	F	Observed frequency (Mc)
3.9452	4	13/2	1.470
3.9452	4	11/2	1.565
3.9452	5	15/2	2.365
3.9452	5	13/2	2.550
3.9452	6	17/2	2.980
7.7917	4	13/2	2.891
7.7917	4	11/2	3.089
7.7917	4	9/2	3.417
7.7917	4	7/2	4.028
7.7917	5	15/2	4.675
7.7917	5	13/2	5.035
7.7917	6	17/2	5.885

Table VII. Fine-structure constants of Nd.

Level	Measured f-s separation (cm^{-1})	Population in beam (%)	Measured g_J value
$^5I_6$	2367	13.4	-1.0715
$^5I_5$	1128	27.5	-0.9002
$^5I_4$	0	50.4	-0.6032

XI. PROMETHIUM-151

A. Introduction

In addition to the spin of 7/2 for Pm^{147} mentioned above, the spins of Pm^{149} and Pm^{151} had also been measured in this Laboratory and found to be 7/2 and 5/2, respectively.[74] It was conjectured that this spin change, upon the addition of the 90th neutron, was of collective origin. Such an effect has been observed in the transition from Eu^{151} to Eu^{153}. The moments of Pm^{151} ought certainly to reflect these phenomena.

Two relevant β-decay measurements have been made. The first,[75] reported before the atomic beam result was known, gave possible spin assignments of 9/2, 1/2-, 3/2±, and 5/2+ to the Pm^{151} ground state. The second pointed out that the log ft value for the decay of 27.5-h Pm^{151} to the Sm^{151} ground state was consistent with spin assignments of 5/2+ and 7/2-, respectively.[76] In the light of the atomic beam work, it seems likely that the parity of the ground state of Pm^{151} is positive.

B. Beam Production

Neutron irradiation of natural neodymium for a period of two days yields roughly the same curie amounts of Pm^{151}, Pm^{149}, and Nd^{147}. The last two are both longer-lived than Pm^{151}. A shorter irradiation fails to produce sufficient activity. A first and only attempt was therefore made with enriched neodymium-150. Aside from the expense involved, this method proved impractical because the enriched material is in the form of the oxide. With the reaction products of a misch metal reduction, old resonances were not reproducible.

These old resonances, on which the spin assignment was based, were obtained by bombarding natural material. To facilitate a hyperfine search, three improvements were made. The bombardment time was extended to four days. The oven volume was doubled to accommodate more material, due consideration being taken of the increased power

requirement. Finally, the counter background was lowered so that a small signal could be detected. This last measure proved somewhat superfluous, for, with the huge beam intensities employed, the machine background swamped the counter background. This background was composed not only of the other isotopes, but also of the $J = 5/2$ level in Pm^{151} itself. The hfs had to be observed in the $J = 7/2$ level for the same reason as in Pm^{147}.

C. Results

Resonances due to both Pm isotopes were followed up in field. Shifted transitions were observed in Pm^{149} up to fields of 85 gauss before it was decided to concentrate exclusively on Pm^{151}. Figures 25 and 26 show α and β resonances in Pm^{151} which are shifted although the field is only 40 gauss. All observations are contained in Table VIII. A comparison of observed and calculated frequencies is made by listing the residuals printed out by the IBM 709 computer. For a total of 11 observations, the value of χ^2 was 0.3. The best-fit values for a and b were

$$a = 358(22)\ \text{Mc},$$
$$b = -778(93)\ \text{Mc}.$$

By comparing these with the corresponding values for Pm^{147}, we may directly deduce values for the moments,

$$\mu = 1.8(2)\ \text{nm},$$
$$Q = 2.9(4)\ \text{b}$$

An interpretation of these moments is given in the next chapter.

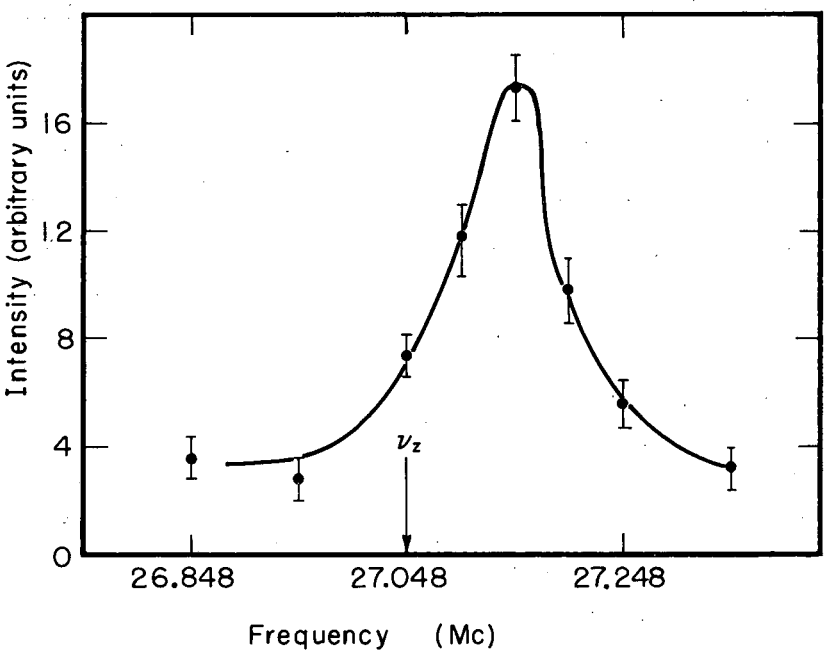

Fig. 25. An α transition in Pm^{151}.

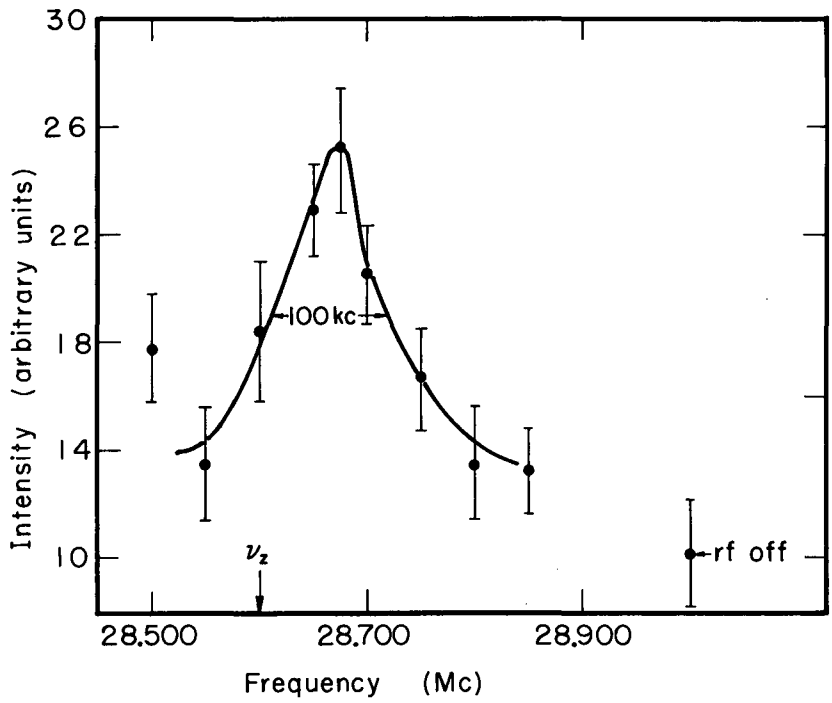

Fig. 26. A β transition in Pm^{151}.

Table VIII. Experimental results in Pm^{151}

H (gauss)	Transition	ν(exp) (Mc/sec)	Residuals (Mc/sec)
40.00	α	27.148	+0.002
40.00	β	28.675	-0.012
60.00	α	40.830	+0.008
60.00	β	43.120	-0.012
60.00	γ	47.135	+0.021
85.00	α	58.050	+0.037
85.00	β	61.275	-0.009
85.00	γ	66.875	-0.021
125.03	α	85.750	-0.011
125.03	β	90.575	+0.001
125.03	γ	98.790	+0.008

XII. INTERPRETATION OF MEASURED SPINS AND MOMENTS

A. Shell Model of Nuclear Structure

The first successful model clarifying the systematics of nuclei, and the one that has served as a point of departure for more sophisticated models, was the nuclear shell model.[77] Its chief success lay in explaining the occurrence of the magic numbers and the nuclear properties associated with them. In its extreme form, the single-particle shell model, the nucleus is characterized by the quantum numbers of the last odd nucleon. This nucleon is assumed to move in a potential that is somewhere between a square well and a harmonic oscillator. The good quantum numbers are, therefore: N, the oscillator quantum number; ℓ, the particle orbital angular momentum; and s, the particle spin angular momentum. To reproduce the magic numbers, a spin-orbit term connecting the particle ℓ and s must be added. Experimental evidence for this term comes from the scattering of polarized protons on helium. Now the particle is characterized by an additional quantum number $j = \ell + s = \ell \pm 1/2$. Borrowing spectroscopic notation, the shell model designates states as $s_{1/2}$, $p_{1/2}$, $p_{3/2}$, etc. The ground-state spin is simply the j value of the odd nucleon and the magnetic moments are the sums of the orbital and spin moments. The latter fall between two limits, the Schmidt lines, corresponding to $j = \ell \pm 1/2$. Once the spin is known, the parity is uniquely determined. Thus the shell model could also predict β-decay selection rules and could calculate log ft data.

B. Weaknesses of the Shell Model

The successes of the shell model pointed up its weaknesses. Not all spins were equal to the j value of the last nucleon. In particular, when more than one nucleon was outside a closed subshell, a coupling to $I = j - 1$ was observed. Also, the magnetic moments deviated considerably from the Schmidt lines, the deviation being quite marked for nuclei with a single nucleon more or less than a filled shell.

But most striking in their disagreement were the quadrupole moments. These were many times the shell-model predictions. Effects

associated with the quadrupole moment, such as isotope shifts and E2 transition probabilities, were also much larger than expected. Finally, the existence of quadrupole moments for odd-neutron nuclei presented a problem. It was therefore suggested that nuclei exhibiting these effects might be permanently deformed.[78] The parameter characterizing the distortion, δ, would, for an ellipsoidal nucleus, be equal to the difference between semimajor and semiminor axes divided by the radius of a sphere of equivalent volume. In terms of the deformation, the quadrupole moment is given by

$$Q = \frac{4}{5} \delta Z R^2 . \tag{50}$$

The factor δZ is, therefore, a measure of the number of nucleons contributing to the distortion. An obvious extension of the shell model to remedy the disagreement between observed and calculated magnetic moments is to admix higher particle configurations corresponding to different moment values. These levels are automatically provided by a nonspherical nucleus, and δZ may then be thought of as the number of admixed shell-model configurations.

C. Collective Model

A simple vector-model treatment of a spheroidal nucleus with an axis of symmetry was proposed.[79] All nucleons in closed shells or subshells are designated as the core. The core can vibrate and rotate, the rotations being of special significance because the coupling of the core to the particle allows a transfer of angular momentum between the two. The nucleon angular momentum precesses about the nuclear axis, which in turn precesses about the total angular momentum. The magnitudes of the different precession frequencies reflect the strength of the various couplings and indicate which vector-model averages are appropriate.

Quantum-mechanically, each coupling corresponds to a term in the Hamiltonian; the stronger the coupling, the more important the term. For a single particle, the Hamiltonian consists of three parts,

$$\mathcal{H} = \mathcal{H}_s(a_{\lambda\mu}) + \mathcal{H}_p(x) + \mathcal{H}_{int}. \tag{51}$$

The first is a function of the deformation parameters and describes the rotational and vibrational modes of the nuclear surface. The second is the energy of the single particle, and can be written

$$\mathcal{H}_p = -\frac{p^2}{2m} + V(x) + C\vec{l}\cdot\vec{s} + D\vec{l}^2, \tag{52}$$

where $V(x)$ is usually taken to be a harmonic oscillator potential. Finally, the coupling of the particle motion to the surface is represented by the third term, and may be written

$$\mathcal{H}_{int} = \delta\hbar\omega \frac{4}{3}\sqrt{\frac{\pi}{5}} r^2 Y_{20}, \tag{53}$$

where ω is the oscillator frequency.

For more than one particle outside of closed shells, the important comparison is between the particle forces and the particle surface coupling. If the latter predominates, the nucleus acquires a permanent cylindrical shape. The particles move independently in the noncentral field so that only the projections of their momenta on the symmetry axis, Ω_p, are good quantum numbers. Levels with $\pm\Omega_p$ are degenerate, so that particles add pairwise, the levels of higher Ω_p being filled first. Thus three particles couple to j-1. If the particle forces are of comparable strength, the particles couple among themselves to a resultant I = j, and this resultant couples to the nuclear axis.

Both these situations are illustrated in Fig. 27. The diagram was taken from a paper by Bohr and Mottelson.[80] In the Pm isotopes, we are dealing with the coupling of three holes in the $g_{7/2}$ shell. Case (a) illustrates the strong-coupling scheme leading to spin 5/2 for Pm^{151}. Case(b) makes plausible a spin of 7/2 for Pm^{147} and Pm^{149}.

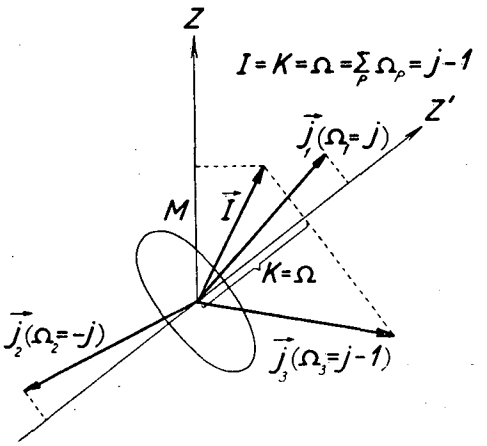

a.

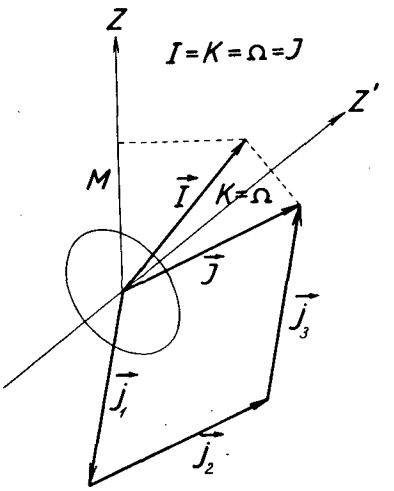

b.

MU-27034

Fig. 27. Three particles in strong and weak coupling.

For weak coupling, one may use perturbation theory, taking as basis functions the shell-model states $|N\ell j m_j\rangle$. As the coupling increases, only N and $m_j = \Omega$ retain their meaning, and it proves convenient to transform to a representation based on Λ and Σ, the projections of ℓ and s, with $\Omega = \Lambda + \Sigma$. These basis functions, denoted by $|N\ell\Lambda\Sigma\rangle$, are the ones used by Nilsson[81] in the strong-coupling model in which he performed an exact diagonalization of the perturbing Hamiltonian,

$$\mathcal{H} - \mathcal{H}_0 = \mathcal{H}_{int} + C\vec{l}\cdot\vec{s} + D\vec{l}^2 . \qquad (54)$$

In the extreme limit of large deformations, the asymptotic quantum-number designation $[N n_z \Lambda]$ is the one appropriate for the states of a pure anisotropic harmonic oscillator. The number of quanta along the symmetry axis is n_z.

D. Discussion of Measured Spins

Pr^{143} is not expected to be a deformed nucleus, so we may attribute its spin to the 59th proton occupying the $g_{7/2}$ shell. This would indicate that the addition of two neutrons to Pr^{141} (I = 5/2) is sufficient to depress the $d_{5/2}$ shell below the $g_{7/2}$.

That the 89th neutron in Nd^{149} so deforms the nucleus that the shell model is inappropriate seems to be true, since no level with j = 5/2 is available. On the other hand, an energy-level diagram for neutron number $82 < N < 126$ shows that a [523] 5/2- state is available for small deformations.[82]

These last authors predict states [523] 7/2- and [523] 5/2- for Ho^{161} and Er^{165}, respectively. Both these predictions are borne out by experiment. They correspond to deformations of $\delta \geq 0.3$ for both nuclei, which should therefore be highly deformed.

E. Magnetic Moments of Pm^{147} and Pm^{149}

On the shell model, the states of the 61st proton in these nuclei are $g_{7/2}$ and $d_{5/2}$. They lead to moments of 1.72 and 4.79. On the collective model, the states would be [404]7/2+ and [413]5/2+. This last assignment is made rather than the one already published,[74] since the evidence has been quoted above for the Pm^{151} ground state having positive parity.

The deformation of the Pm^{147} nucleus as estimated below from the quadrupole moment and from the spin is too small for Nilsson's wave functions to apply. It is interesting, however, to speculate on the origin of the discrepancy whereby the measured moment deviates by almost 100% from the Schmidt value. The interaction Hamiltonian(53) can mix in states of the same Ω and parity, but with N and ℓ differing by 2. Such states arise from the $i_{13/2}$ and $i_{11/2}$ levels. As zero-order wave functions, we may take the Nilsson functions in the limit of zero deformation, for then they must be identical with the shell-model functions. We find that the states designated as [633]7/2+, [624]7/2+, and [613]7/2+ can all be admixed. The matrix elements for the operator r^2Y_{20} can be evaluated by using formalae given by Nilsson. Since to this approximation the magnetic-moment operator is diagonal between the ground state and the excited states, the effect is to increase the calculated moment by 0.01%.

For Pm^{151} the Nilsson wave function for a deformation of 0.3 is

$$0.929 \mid 442+\rangle + 0.211 \mid 422+\rangle + 0.302 \mid 443-\rangle .$$

This leads to a dipole moment of 3.44 nm, in agreement with the measured value.

F. Quadrupole Moments

Quadrupole moments, like magnetic moments, are defined as expectation values and hence should be sensitive to the wave functions. The sign of the quadrupole moment, however, depends only on whether nucleus is an oblate or prolate spheroid and this in turn, depends on whether

the shell is less or more than half filled. Accordingly, an assignment to $g_{7/2}$ state correctly predicts a positive quadrupole moment for Pm^{147}. The quadrupole moment for $(d_{5/2})^3$, on the other hand, should vanish! Even for Pm^{147}, the shell model gives a quadrupole moment of 0.08 b, whereas the measured value is ten times as great.

Expression (50) for the moment of a deformed nucleus is referred to as the intrinsic quadrupole moment. It must be multiplied by a projection factor, to take account of the rotation, which is approximately unity for weak coupling and approaches the limit (I/I+1) (2I-1/2I+3) for strong coupling.

If Pm^{147} is assumed weakly coupled with $\delta = 0.05$, a quadrupole moment of 1.4 b is obtained. This is in fair agreement with experiment. Since all the previous evidence points to a strong coupling for Pm^{151}, we can assume $\delta = 0.3$ and find 2.9 b. The agreement with experiment further confirms that the nucleus of Pm^{151} is highly deformed.

APPENDIX I.

Hund's Rule for Equivalent Electrons

Hund's Rule for equivalent electrons states that the term of maximum S and among these the term of maximum L is lowest in energy. The proof rests on the exclusion principle, which in its most general form states that the total wave function must be antisymmetric. The Coulomb repulsion between electrons raises the energy. Thus that state will be lowest in energy which has the electrons farthest apart spatially or in which the wave functions describing the electrons do not overlap. If ϕ_1 and ϕ_2 are two wave functions, then the antisymmetric combination

$$\phi_1(1)\,\phi_2(2) - \phi_1(2)\phi_2(1)$$

clearly vanishes as $\phi_1 \rightarrow \phi_2$. This combination goes with the symmetric spin function corresponding to all spins up and maximum S. It is interesting to note that for $(1) \rightarrow (2)$ the antisymmetric combination again vanishes, corresponding to the coordinates $x_1\ y_1\ z_1$ of electron No. 1 approaching $x_2\ y_2 z_2$ of electron No. 2. The second part of Hund's Rule concerning maximum L is not easily visualized in the many-electron case, although a plausibility argument can be made for two electrons by considering the overlapping of orbits.

APPENDIX II.

Tensor Operator Forms for Magnetic Dipole and Electric Quadrupole Interaction.

For a non-s electron the magnetic dipole interaction can be written[13]

$$\mathcal{H}_{mgs} = \frac{2\mu_0\mu_N g_I}{I} \left\langle \frac{1}{r^3} \right\rangle \left[\underset{\sim}{\ell} - \underset{\sim}{s} + \frac{3\underset{\sim}{r}(\underset{\sim}{r}\cdot\underset{\sim}{s})}{r^2} \right] \cdot \underset{\sim}{I} .$$

In terms of the quantities

$$c_q^{\,k} = (-1)^q \sqrt{\frac{(k-q)!}{(k+q)!}}\; p_k^{\,q}(\cos e)\, e^{iq\phi} ,$$

we can write

$$\frac{3\underset{\sim}{r}(\underset{\sim}{r}\cdot\underset{\sim}{s})}{r^2} = \frac{3(\underset{\sim}{s}\cdot\underset{\sim}{r})\underset{\sim}{r}}{r^2} = 3(\underset{\sim}{s}\cdot\underset{\sim}{c}')\underset{\sim}{c}' = -3\sqrt{3}\,(\underset{\sim}{s}\,\underset{\sim}{c}')^0 c' ,$$

where the bracket in the last expression is read "vector $\underset{\sim}{s}$ and operator $\underset{\sim}{c}'$ coupled up to zero." The last expression is simplified by uncoupling $\underset{\sim}{s}$ from $\underset{\sim}{c}'$ and recoupling $\underset{\sim}{c}'$ to $\underset{\sim}{c}'$. We have then the two different sequences in which three angular momenta can be coupled and should anticipate the 6-j symbol. In fact,

$$-3\sqrt{3}\,(\underset{\sim}{s}\,\underset{\sim}{c}')^0\,\underset{\sim}{c}' = -3\sqrt{3}\sum_k \left((11)0, 1, 1 \,|\, 1, (11)k, 1 \right)(\underset{\sim}{s}(\underset{\sim}{c}'\underset{\sim}{c}')^k)' .$$

The bracket contains the information that two vectors, tensors of rank 1, formerly coupled to each other with 0 resultant rank, dot product, and then coupled to another vector to form a vector, are now uncoupled. The last two vectors are now coupled to rank k and this k is combined with the first vector to produce the same resultant as initially. Now,

$$\left((11)0,\ 1, 1 \,|\, 1,\ (11)k,\ 1\right) = \sqrt{2k+1} \begin{Bmatrix} 1 & 1 & k \\ & & \\ 1 & 1 & 0 \end{Bmatrix} = \frac{1}{3}(-1)^k \sqrt{2k+1},$$

and the general result,

$$(\underset{\sim}{c}^{k_1}\,\underset{\sim}{c}^{k_2})^k = (-1)^k \sqrt{2k+1}\begin{pmatrix} k_1 & k & k_2 \\ 0 & 0 & 0 \end{pmatrix}\underset{\sim}{c}^k ,$$

provided the c^k refer to the same particle, means that with $k_1 = k_2 = 1$, k can have only the values 0 and 2, (vector product of two equal vectors vanishes),

$$(\underset{\sim}{c}'\,\underset{\sim}{c}')^0 = -\sqrt{1/3}\,\underset{\sim}{c}^0 = -\sqrt{1/3}, \quad (\underset{\sim}{c}'\,\underset{\sim}{c}')^2 = \sqrt{2/3}\,\underset{\sim}{c}^2 .$$

Therefore

$$-3\sqrt{3}\,(\underset{\sim}{s}\,\underset{\sim}{c}')^0\underset{\sim}{c}' = -3\sqrt{3}\left[\frac{1}{3}\left(-\sqrt{1/3}\right)\underset{\sim}{s} + \sqrt{5/3}\sqrt{2/3}\,(\underset{\sim}{s}\,\underset{\sim}{c}^2)^1\right] = \underset{\sim}{s} - \sqrt{10}\,(\underset{\sim}{s}\,\underset{\sim}{c}^2)^1 ,$$

and

$$\mathcal{H}_{magn} = \frac{2\mu_0\mu_N g_I}{I}\left\langle\frac{1}{r^3}\right\rangle\left[\underset{\sim}{\ell} - \sqrt{10}\,(\underset{\sim}{s}\,\underset{\sim}{c}^2)^1\right]\cdot\underset{\sim}{I}.$$

For the electrostatic interaction between the nucleons and electrons we write[15]

$$\mathcal{H}_{elec} = \sum_{\ell, N}\frac{e^2}{|\underset{\sim}{r}_\ell - \underset{\sim}{r}_N|} = \sum_{e, N, k} e^2\,\frac{r_N^k}{r_e^{k+1}}\,P_k(\cos\theta_{eN}) ,$$

where e refers to the electron and N to the nucleon (proton). If we consider only the quadrupole term in the expansion and use the spherical harmonic addition theorem, we may write

$$\mathcal{H}_{elec} = \sum_{e, N, q}(-1)^q\,\frac{r_N^2}{r_e^3}\,c_q^2(\theta_e, \phi_e)\,c_{-q}^2(\theta_N, \phi_N) .$$

Appendix III. The fpc used in computing the spin-orbit interaction.

	Offspring				
Parents	$^6H(110)(11)$	$^4G(210)(20)$	$^4G(210)(21)$	$^4G(210)(30)$	$^4G(111)(20)$
$(110)(910)^5F$	$-\sqrt{\frac{1}{10}}$	$\frac{1}{2}\sqrt{\frac{7}{8}}$	0	0	$\frac{1}{2^2}\sqrt{\frac{1}{2}}$
$(111)(20)^5D$	$-\sqrt{\frac{2}{3\cdot 7}}$	$\frac{1}{2^2\cdot 7}\sqrt{\frac{5\cdot 11}{2\cdot 3}}$	$\frac{1}{2\cdot 3\cdot 7}\sqrt{\frac{13}{2}}$	$\frac{1}{2\cdot 3}\sqrt{\frac{11}{2}}$	$-\frac{1}{2^2}\sqrt{\frac{5\cdot 11}{2\cdot 3\cdot 7}}$
$(111)(20)^5G$	$-\sqrt{\frac{3\cdot 13}{2\cdot 7\cdot 11}}$	$-\frac{5}{2^2\cdot 7}\sqrt{\frac{5}{2\cdot 11}}$	$\frac{1}{7}\sqrt{\frac{2\cdot 13}{3}}$	$\frac{1}{2}\sqrt{\frac{2}{3\cdot 11}}$	$\frac{5}{2^2}\sqrt{\frac{5}{2\cdot 7\cdot 11}}$
$(111)(20)^5I$	$\sqrt{\frac{7\cdot 13}{3\cdot 5\cdot 11}}$	$\frac{1}{2^2}\sqrt{\frac{13}{2\cdot 3\cdot 11}}$	$\frac{1}{2\cdot 3}\sqrt{\frac{5}{2}}$	$-\frac{1}{2\cdot 3}\sqrt{\frac{5\cdot 13}{2\cdot 11}}$	$-\frac{1}{2^2}\sqrt{\frac{7\cdot 13}{2\cdot 3\cdot 11}}$

Appendix IV. Table of fpc used in calculating matrix of U^2.

Parents f^3	Offspring f^4 (110)(11) 3H	(211)(20) 3G	(211)(21) 3G	(211)(30) 3G	(111)(20) 5G
$(110)(10)^4F$	$\sqrt{\frac{1}{2\cdot 3\cdot 5}}$	$\frac{1}{2}\sqrt{\frac{7}{6}}$	0	0	$\frac{1}{2}\sqrt{\frac{1}{2}}$
$(111)(20)^4D$	$-\frac{1}{3}\sqrt{\frac{2}{7}}$	$\frac{1}{6\cdot 7}\sqrt{\frac{5\cdot 11}{2}}$	$\frac{1}{21}\sqrt{\frac{13}{2\cdot 3}}$	$\frac{1}{3}\sqrt{\frac{11}{6}}$	$-\frac{1}{2}\sqrt{\frac{5\cdot 11}{2\cdot 3\cdot 7}}$
$(111)(20)^4G$	$-\sqrt{\frac{13}{2\cdot 7\cdot 11}}$	$-\frac{5}{14}\sqrt{\frac{5}{2\cdot 3\cdot 11}}$	$\frac{2}{3\cdot 7}\sqrt{2\cdot 13}$	$\frac{1}{3}\sqrt{\frac{2}{11}}$	$\frac{5}{2}\sqrt{\frac{5}{2\cdot 7\cdot 11}}$
$(111)(20)^4I$	$\frac{1}{3}\sqrt{\frac{7\cdot 13}{5\cdot 11}}$	$\frac{1}{6}\sqrt{\frac{13}{2\cdot 11}}$	$\frac{1}{3}\sqrt{\frac{5}{2\cdot 3}}$	$-\frac{1}{3}\sqrt{\frac{5\cdot 13}{2\cdot 3\cdot 11}}$	$-\frac{1}{2}\sqrt{\frac{7\cdot 13}{2\cdot 3\cdot 11}}$
$(210)(11)^2P$	0	$\frac{1}{7}\sqrt{\frac{11}{3}}$	$\frac{1}{28}\sqrt{5\cdot 13}$	0	0
$(210)(11)^2H$	0	$-\frac{1}{21}\sqrt{5\cdot 13}$	$\frac{1}{28}\sqrt{3\cdot 11}$	0	0
$(210)\ (20)^2D$	$\frac{1}{21}$	$\frac{2}{21}\sqrt{\frac{5\cdot 11}{7}}$	$-\frac{5}{2^2\cdot 3\cdot 7}\sqrt{\frac{13}{3\cdot 7}}$	$\frac{1}{3}\sqrt{\frac{11}{3\cdot 7}}$	0
$(210)(20)^2G$	$\frac{1}{2\cdot 7}\sqrt{\frac{13}{11}}$	$-\frac{2\cdot 5}{7}\sqrt{\frac{5}{3\cdot 7\cdot 11}}$	$-\frac{5}{3\cdot 7}\sqrt{\frac{13}{7}}$	$\frac{2}{3}\sqrt{\frac{1}{7\cdot 11}}$	0
$(210)(20)^2I$	$-\frac{1}{6}\sqrt{\frac{2\cdot 13}{5\cdot 11}}$	$\frac{2}{3}\sqrt{\frac{13}{7\cdot 11}}$	$-\frac{5}{2^2\cdot 3}\sqrt{\frac{5}{3\cdot 7}}$	$-\frac{1}{3}\sqrt{\frac{5\cdot 13}{3\cdot 7\cdot 11}}$	0
$(210)\ (21)^2D$	$-\frac{3}{2\cdot 7}\sqrt{\frac{3}{11}}$	$-\frac{2}{3\cdot 7}\sqrt{\frac{3\cdot 5}{7}}$	$-\frac{13}{3\cdot 7}\sqrt{\frac{11}{7\cdot 13}}$	$\frac{5}{2\cdot 3}\sqrt{\frac{1}{7}}$	0
$(210)(21)^2F$	$\frac{1}{4}\sqrt{\frac{2\cdot 3}{5\cdot 11}}$	$-\frac{2}{3}\sqrt{\frac{3}{2\cdot 7\cdot 11}}$	$\frac{1}{2\cdot 3}\sqrt{\frac{5\cdot 13}{2\cdot 7}}$	$\frac{7}{3}\sqrt{\frac{5}{2\cdot 7\cdot 11}}$	0
$(210)(21)^2G$	$-\frac{3}{28}\sqrt{\frac{2\cdot 3}{5}}$	$-\frac{1}{7}\sqrt{\frac{2\cdot 13}{7}}$	$\frac{23}{2\cdot 3\cdot 7}\sqrt{\frac{3\cdot 11}{2\cdot 5\cdot 7}}$	$-\frac{1}{3}\sqrt{\frac{3\cdot 13}{2\cdot 5\cdot 7}}$	0
$(210)(21)^2H$	$\frac{1}{2}\sqrt{\frac{1}{5}}$	$-\frac{2}{3}\sqrt{\frac{1}{7}}$	$-\frac{2}{3}\sqrt{\frac{3\cdot 11}{5\cdot 7\cdot 13}}$	$\frac{1}{2}\sqrt{\frac{7}{3\cdot 5}}$	0
$(210)(21)^2K$	$\frac{1}{2}\sqrt{\frac{3}{11}}$	$2\sqrt{\frac{5}{3\cdot 7\cdot 11}}$	$2\sqrt{\frac{1}{7\cdot 13}}$	$3\sqrt{\frac{1}{7\cdot 11}}$	0
$(210)(21)^2L$	$-\frac{1}{2}\sqrt{\frac{17}{5\cdot 11}}$	0	0	0	0
$(100)(10)^2F$	$+\frac{1}{2}\sqrt{\frac{5}{3}}$	0	0	0	0

Appendix V. The 9-j symbols appearing in Eq. (43).

$$\begin{Bmatrix} \frac{5}{2} & \frac{5}{2} & 1 \\ 5 & 5 & 2 \\ \frac{7}{2} & \frac{7}{2} & 1 \end{Bmatrix} = \frac{19}{2^2 \cdot 3^2 \cdot 5 \cdot 7} \sqrt{\frac{3 \cdot 13}{5 \cdot 11}}$$

$$\begin{Bmatrix} \frac{5}{2} & \frac{3}{2} & 1 \\ 5 & 4 & 2 \\ \frac{7}{2} & \frac{7}{2} & 1 \end{Bmatrix} = \frac{11}{3^2 \cdot 5} \sqrt{\frac{1}{2 \cdot 5 \cdot 7}}$$

$$\begin{Bmatrix} \frac{3}{2} & \frac{3}{2} & 1 \\ 4 & 4 & 2 \\ \frac{7}{2} & \frac{7}{2} & 1 \end{Bmatrix} = \frac{17}{2 \cdot 3^3 \cdot 5 \cdot 7} \sqrt{\frac{11}{5}}$$

ACKNOWLEDGMENTS

It is with delight that I take this opportunity to thank the many individuals who have made this work possible:

My family, my parents and brothers, for their warm friendship and confidence in me.

Professor William A. Nierenberg for his support.

Dr. Richard Marrus for his invaluable encouragement and guidance.

Professor Howard Shugart for his kind interest.

Dr. Brian Judd for his patient and inspiring instruction.

Mr. Douglas MacDonald for his ready aid with problems of apparatus and design.

Dr. Seymour Alpert, Isaac Maleh, and Matthew White for their graciously extended help in the runs.

The health chemists, in particular R. McCracken, H. Adams, K. Voice, M. Lombardo, and P. Van de Mark, for their continuous cooperation and concern.

REFERENCES

1. E. M. Condon and G. H. Shortley, Theory of Atomic Spectra (Cambridge University Press, 1957).
2. P. A. M. Dirac, Quantum Mechanics (Oxford University Press, 1959).
3. B. R. Judd (Lawrence Radiation Laboratory), private communication.
4. J. P. Elliot, B. R. Judd, and W. A. Runciman, Proc. Roy. Soc. (London) A240, 509 (1957).
5. P. F. A. Klinkenberg, Physica 13, 1 (1947).
6. W. Pauli, Naturwiss enschaften 12, 741 (1924).
7. E. Fermi, Z. Physik 60, 320 (1930).
8. J. Hargreaves, Proc. Roy. Soc. (London) A124, 568 (1929); A127, 141, 407 (1930).
9. S. Goudsmit, Phys. Rev. 37, 663 (1931).
10. R. A. Ferrel, Am. J. Phys. 28, 484 (1960).
11. C. Schwartz, Phys. Rev. 97, 380 (1955).
12. H. B. G. Casimir, On the Interaction Between Atomic Nuclei and Electrons (Teyler's Tweede Genootschap, Haarlem, 1936).
13. Norman F. Ramsey, Nuclear Moments (John Wiley and Sons, Inc., New York, 1953).
14. J. C. Hubbs, W. A. Nierenberg, R. Marrus, and J. L. Worcester, Phys. Rev. 109, 390 (1958).
15. A. R. Edmonds, Angular Momentum in Quantum Mechanics (Princeton University Press, 1957).
16. Norman F. Ramsey, Molecular Beams (Oxford University Press, 1956).
17. R. Marrus (Lawrence Radiation Laboratory), private communication.
18. S. Millman, I. I. Rabi, and J. R. Zacharias, Phys. Rev. 53, 384 (1938).
19. I. I. Rabi, J. M. B. Kellogg, and J. R. Zacharias, Phys. Rev. 46, 157 (1934).
20. I. I. Rabi, J. R. Zacharias, S. Millman, and P. Kusch, Phys. Rev. 53, 318 (1938).

21. J. R. Zacharias, Phys. Rev. 61, 270 (1942).

22. Gilbert O. Brink, Nuclear Spins of Thallium-197, Thallium-198m Thallium-199, and Thallium-204 (thesis, UCRL-3642, June 1957).

23. Joseph Winocur, Nuclear and Electronic Ground State Properties of Pa^{233} Am^{241}, and 16 h Am^{242} (thesis, UCRL-9174, April 1960).

24. Seymour S. Alpert, The Moments, Spins, and Hyperfine Structures of the Radioactive Isotopes, I^{133}(21-h), Nd^{141}(2.5-h), Eu^{152} (130yr), and Bi^{210}(5-day), (thesis, UCRL-9850, September 1961).

25. I. I. Rabi, Phys. Rev. 51, 652 (1937).

26. P. Kusch and V. W. Hughes, Atomic and Molecular Beam Spectroscopy, in Handbuch der Physik Vol. 37 (Springer 1959).

27. M. N. Hack, Phys. Rev. 104, 84 (1956);
H. Salwen, Phys. Rev. 99, 1274 (1955).

28. I. I. Rabi, N. F. Ramsey, and J. Schwinger, Revs. Modern Phys. 26, 167 (1954).

29. P. Kusch and H. Taub, Phys. Rev. 75, 1477 (1949).

30. H. Frauenfelder, Helv. Phys. Acta 23, 347 (1950).

31. R. Marrus, W. A. Nierenberg, and J. Winocur, Phys. Rev. 120, 1429 (1960).

32. R. A. Fisher, Statistical Methods for Research Workers (Hafner, New York, 1958).

33. H. Garvin, T. M. Green, E. Lipworth, and W. A. Nierenberg, Phys. Rev. 116, 393 (1959).

34. H. E. Suess, Phys. Rev. 81, 1071 (1951).

35. J. A. Marinsky , L. E. Glendenin, and C. D. Coryell, J. Am. Chem. Soc. 69, 2781 (1947).

36. L. M. Langer, J. W. Motz, and H. C. Price, Jr., Phys. Rev. 77, 798 (1950).

37. E. J. Konopinski and L. M. Langer, The Experimental Clarification of the Theory of β-Decay, Ann. Rev. Nuclear Sci. 2, 261 (1953).

38. D. A. Shirley, J. F. Schooley, and J. O. Rasmussen, Phys. Rev. 121, 558 (1961).

39. A. Cabezas, I. Lindgren, E. Lipworth, R. Marrus, and M. Rubinstein, Nuclear Phys. 20, 509 (1960).
40. P. F. A. Klinkenberg and F. S. Tomkins, Physica 26, 103 (1960).
41. H. J. Stapleton, C. D. Jeffries, and D. A. Shirley, Phys. Rev. 124, 1455 (1961).
42. G. Racah, Phys. Rev. 76, 1352 (1949).
43. B. G. Wybourne, J. Chem. Phys. 35, 334 (1961).
44. W. F. Meggers, B. F. Scribner, and W. R. Bozman, Bur. Standards J. Research 46, 85 (1951).
45. B. R. Judd (Lawrence Radiation Laboratory), private communication.
46. B. R. Judd, Proc. Roy. Soc. (London) A228, 126 (1955).
47. B. G. Wybourne, J. Chem. Phys. 35, 340 (1961).
48. B. R. Judd and I. Lindgren, Phys. Rev. 122, 1802 (1961).
49. B. R. Judd (Lawrence Radiation Laboratory), private communication.
50. B. R. Judd, Lawrence Radiation Laboratory Report UCRL-9868, September 1961.
51. L. S. Goodman, W. J. Childs, R. Marrus, I. P. K. Lindgren, and A. Y. Cabezas, Bull. Am. Phys. Soc. II 5, 344 (1960).
52. W. J. Childs and L. S. Goodman, Phys. Rev. 122, 591 (1961).
53. T. H. Handley and E. L. Olson, Phys. Rev. 93, 524 (1954).
54. J. W. Mihelich and B. Harmatz, Phys. Rev. 106, 1232 (1957).
55. A. Y. Cabezas, Electronic and Nuclear Properties of Some Radioactive Rare Earth Elements (thesis), UCRL-9346, Aug. 1960.
56. A. Y. Cabezas, I. P. K. Lindgren, and R. Marrus, Bull. Am. Phys. Soc. 5, 343 (1960).
57. K. F. Smith and I. J. Spalding, Proc. Roy. Soc. (London) A265, 133 (1961).
58. B. Bleaney and H. E. D. Scovil, Proc. Phys. Soc. (London) 64A, 204 (1951).
59. I. Maleh (Lawrence Radiation Laboratory), private communication.
60. F. D. S. Butement, Proc. Phys. Soc. (London 63A, 775 (1950); D. N. Kundu, J. D. Service, M. L. Pool, and G. E. Boyd, Phys. Rev. 60, 722 (1941).

61. N. Rosen, G. R. Harrison, and J. R. MacNally, Phys. Rev. 60, 722 (1941).

62. P. Schuurmanns, Physica 12, 589 (1946);
W. F. Meggers, Science 105, 514 (1947).

63. H. Lew, Phys. Rev. 91, 619 (1953).

64. R. Marrus, A. Y. Cabezas, I. Lindgren, and W. A. Nierenberg, Bull. Am. Phys. Soc. 7, 25 (1962).

65. M. L. Pool and J. D. Kurbatoc, Phys. Rev. 63, 463 (1943);
F. Joliot, Compt. rend. 218, 489 (1944);
O. Hahn and F. Strassmann, Naturwiss enschaften 31, 499 (1943).

66. N. E. Ballou, Discovery of 14d Pr in Fission, in Radiochemical Studies: The Fission Products, C. D. Coryell and N. Sugarman, Eds. (McGraw-Hill Book Company, Inc., New York, 1951).

67. H. W. Wright, E. I. Wyatt, S. A. Reynolds, W. S. Lyson, and T. H. Handley, Nuclear Sci. Eng. 2, 427 (1957).

68. D. F. Pippard, G. W. Mason, and S. W. Moline, J. Inorg. Nuclear Chem. 5, 148 (1957).

69. P. W. Martin, M. K. Brice, J. M. Cork, and S. B. Burson, Phys. Rev. 101, 182 (1956).

70. E. Kondaiah, Phys. Rev. 83, 471 (1951).

71. W. C. Rutledge, J. M. Cork, and S. B. Burson, Phys. Rev. 86, 775 (1952).

72. F. H. Spedding (Iowa State University), private communication.

73. P. Schuurmanns, Physica 11, 419 (1946).

74. A. Y. Cabezas, I. Lindgren, and R. Marrus, Phys. Rev. 122, 1796 (1961).

75. L. C. Schmid and S. B. Burson, Phys. Rev. 115, 178 (1959).

76. R. Chery, J. Phys. radium 22, 665 (1961).

77. Maria Goeppert Mayer and J. Hans D. Jensen, Elementary Theory of Nuclear Shell Structure (John Wiley and Sons, Inc., New York, 1960).

78. J. Rainwater, Phys. Rev. 79, 432 (1950).

79. A. Bohr, Phys. Rev. 81, 134 (1951).

80. A. Bohr and B. R. Mottelson, Kgl. Danske Videnskab. Selskab, Mat.-fys. Medd. 27, 16 (1953).

81. S. G. Nilsson, Kgl. Danske, Videnskab. Selskab, Mat.-fys. Medd. 29, 16 (1955).

82. B. R. Mottelson and S. G. Nilsson, Kgl. Danske Videnskab. Selskab, Mat.-fys. Skrifter, 1, 8 (1959).